Pergamon

Int. J. Solids Structures Vol. 32, No. 13, pp. 1807–1857, 1995

0020-7683/95 $9.50 + .00

0020-7683(94)00232-0

GREEN FUNCTIONS FOR A HALF CIRCULAR CRACK IN HALF INFINITE SPACE UNDER NORMAL LOADING

GUIDO DHONDT
MTU Motoren- und Turbinen-Union München GmbH, Postfach 50 06 40, 80976 München, Germany

(*Received* 9 *March* 1994; *in revised form* 17 *September* 1994)

Abstract—The stress intensity factor distribution along a half circular crack in a half infinite space due to a point force acting normal to the crack faces, is derived by means of the alternating method. Special attention is given to the solution near the free surface. Asymptotic expressions are derived for the zero and first iteration of the stresses, displacements and the stress intensity factor. It is proven that after one iteration the stress intensity factor distribution tends to zero very near to the free surface, leaving an extremely small pressure zone at the free surface. The results are compared with other recent theoretical research and experimental evidence. Finally, for a matrix of about 60 representative point load positions the K-distribution after one iteration is given explicitly using B-splines.

1. INTRODUCTION

At a straight boundary, cracks frequently take a near half circular shape. This is particularly true for cracks in the bore region of aircraft engine disks. Being able to calculate the precise stress intensity factor distribution (K) along such a crack and to predict its propagation is of vital importance to engine health monitoring systems. Whereas the K distribution in the depth of a half circular crack is relatively well known, for instance by using numerical techniques such as the Finite Element Method, there is no straightforward solution at the free surface.

In a first approximation the crack under consideration can be modelled by a half circular crack in a half infinite space. The material is assumed to be homogeneous and linear elastic. One of the first treatments of this problem was given by Smith *et al.* (1967a, b). Using the alternating technique the K-distribution under a constant load was found to increase towards some constant value at the free surface. However, a more thorough analysis by Hartranft and Sih (1973) suggested that the K-distribution, though at first increasing from the deepest point of the crack front towards the free surface, decreases quite sharply at the free surface. They also applied the alternating method, using the findings of Muki (1960) for the full circular crack solution in infinite space. The main difference with the previous approach of the problem was the separate numerical treatment of the stress singularities occurring at the crack front. The conjecture was made that the K-factor distribution might even tend to zero at the free surface.

Using the alternating method, analytical progress in solving the half circular problem depends heavily on the availability of a simple solution (stresses, displacements and K-distribution) for the full circular problem. A couple of years ago a marvellously simple solution for the Green functions for a full circular crack was developed (Fabrikant, 1988). The solution is explicit, containing no series expansions and involving no functions more complicated than a square root or exponential. This solution is used in the present article to analyse the Green function for a half circular crack by the alternating method.

Though the calculations were done numerically, every effort was spent to use analytical asymptotic expansions near the intersection of the crack front with the free surface. Indeed, the simplicity of the full crack solution made it possible to derive analytical expressions for the leading behaviour of the zero and first iteration values of stresses, displacements and K-distribution. The first iteration reveals that the K-factor indeed tends to zero in a logarithmic way very near the free surface, leaving an extremely small pressure zone at the

free surface (10^{-16} [L] for a crack of 1 [L], where [L] represents the dimension of length). The derivation of the analytical expressions for the subsequent iterations would require the solution of the non-linear contact problem created by this crack closure. This formidable task was not attempted. However, it is proven that the effect of this small pressure zone on the solution in subsequent iterations will be locally limited.

A zero for the K-distribution at or near the free surface agrees with previous analytical findings. Recently, it was shown by the finite element technique (Becker, 1989) that the usual crack front stress singularity of $r^{-0.5}$ decreases at a free surface to about $r^{-0.4}$. Moreover, experimental evidence systematically reveals a retreating of the crack front very near the free surface. Although this has frequently been attributed to plasticity effects at the free surface, the present study suggests that a basic linear elastic surface phenomenon might also be involved.

All theoretical derivations in the present article have been collected in Appendices in order not to cloud the main line of thought.

2. ALTERNATING METHOD

In order to find the stress intensity factor along a half circular crack in a half infinite space the so-called alternating method will be applied (Hartranft and Sih, 1973; Kantorovich and Krylov, 1964). The basic idea of this method is to find a solution to the governing equations of the problem at hand satisfying only part of the boundary conditions. This should be an easier task than the original one. Next, another solution to the governing equations is superimposed making sure that the boundary conditions which were not yet satisfied are fulfilled. However, this latter solution usually destroys the fulfilment of the boundary conditions which were satisfied by the first solution. So, the first solution must be applied again. This procedure is repeated until a convergent solution is obtained. For the solution of the half circular crack problem in a half infinite space the solution of the full circular crack in infinite space will be taken as starting solution.

Suppose (Fig. 1) that the K-factor distribution along a half circular crack in a half infinite space due to a point force acting on the crack faces is asked for. In the zero iteration the solution $K(\phi)_0$ for two symmetric point forces on a circular crack in infinite space is taken. However, this will result in a normal stress $(\sigma_y)_1$ on the xz-plane.

Since this plane should be stress free, the first iteration starts with solving the problem of a half infinite space without crack whose boundary plane is loaded with $-(\sigma_y)_1$. This leads to a normal stress $(\sigma_z)_2$ on the crack surfaces. Since these should be stress free apart from the point load, the second part of the first iteration again involves the problem of a circular crack in infinite space, loaded with $-(\sigma_z)_2$ for $y \geqslant 0$ and its symmetric equivalent for $y < 0$, leading to a $K(\phi)_1$ stress intensity factor distribution and a $(\sigma_y)_3$ normal stress on the xz-plane. At this point the second iteration starts. This process is continued until after iteration i $(\sigma_y)_{2i+1}$ is deemed small enough. Then $K(\phi)$ takes the value:

$$K(\phi) = \sum_{j=0}^{i} K(\phi)_j. \tag{1}$$

Summarizing the solution of two problems is needed for the present application:

1. The K-solution, stresses and (as will be shown later) displacements in infinite space due to a circular crack loaded by normal forces. The corresponding Green function was derived for transversely isotropic elastic materials in a particularly simple form by Fabrikant (1988). In Appendix A the formulae for isotropic elastic materials are derived by a limiting process.
2. The stresses in a half infinite space due to normal loading forces on the bounding surface. The corresponding Green function can be found in the literature [e.g. Timoshenko and Goodier (1970) for the solution in polar coordinates]. In Appendix C the formulae are derived as a special case of the circular crack problem solution given by Fabrikant.

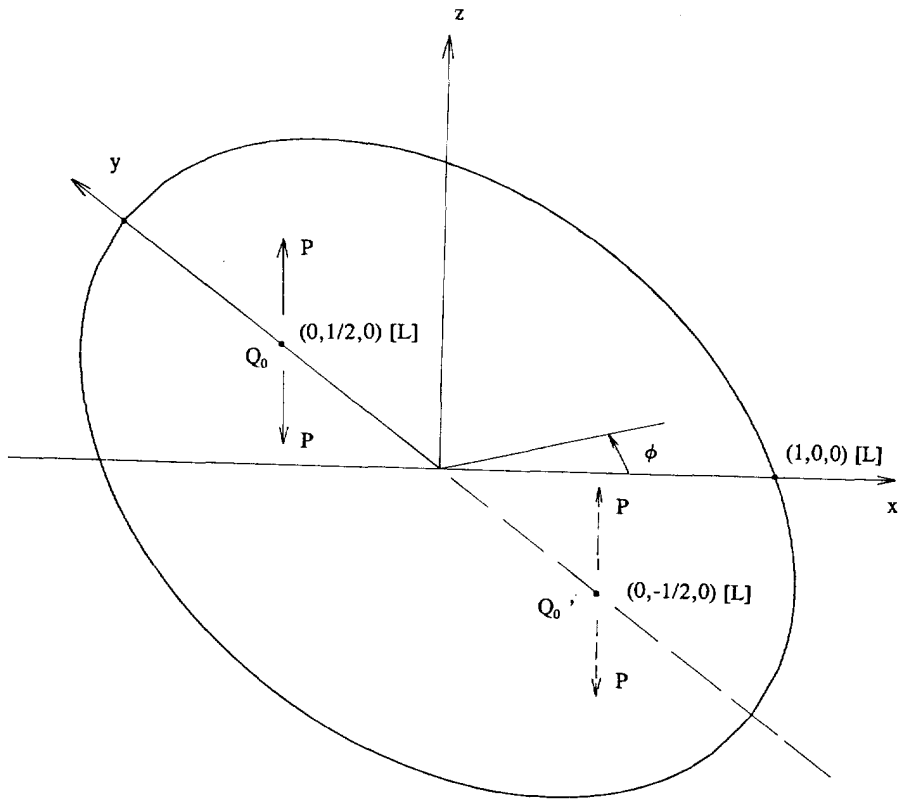

Fig. 1. Point force in the interior of a half space.

Due to the occurrence of singularities at the crack front the problem is more complicated than it looks. Following Hartranft and Sih (1973), the singularities were extracted and analysed separately. In this respect the relatively uncomplicated solution to the circular crack problem given by Fabrikant was of great help.

3. POINT FORCE IN THE INTERIOR OF THE HALF SPACE

Suppose a unit point force acts at the point $Q_0(0, 1/2, 0)$ [L]. The free surface corresponds to $y = 0$ (Fig. 1) and the radius of the crack $a = 1$ [L]. The units of force are denoted by [F], the units of length by [L]. Poisson's coefficient $\nu = 0.3$ and Young's modulus $E = 210{,}000$ [F]/[L]^2 is assumed throughout.

Zero iteration

The K-value along the crack front due to two symmetric point forces at Q_0 and Q_0' can be determined using the Green function given by Gao and Rice (1987). It is worthwhile pointing out that the solution given by Fabrikant (1988) is $(2\pi)^{1/2}$ smaller due to a different K definition. Here the former (and usual) definition will be taken. It leads to

$$K(\phi)_0 = \frac{P}{\pi\sqrt{\pi a}}\sqrt{a^2-\beta^2}\left(\frac{1}{r_1^2}+\frac{1}{r_2^2}\right) \tag{2}$$

where

$$r_{1,2}^2 = a^2+\rho_0^2-2a\rho_0\cos(\phi\pm\phi_0). \tag{3}$$

ϕ denotes the location along the circular crack at which the K-factor is calculated, P is the point force, a is the radius of the crack and the location of Q_0 is given by (ρ_0, ϕ_0) in polar

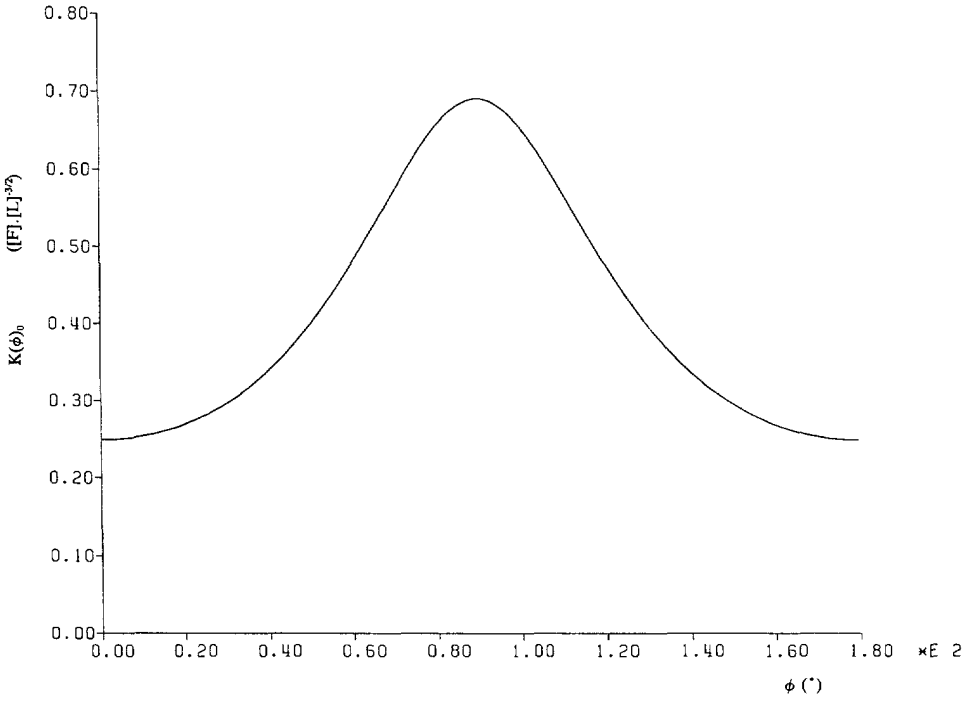

Fig. 2. K-distribution along a circular crack in infinite space due to a point force.

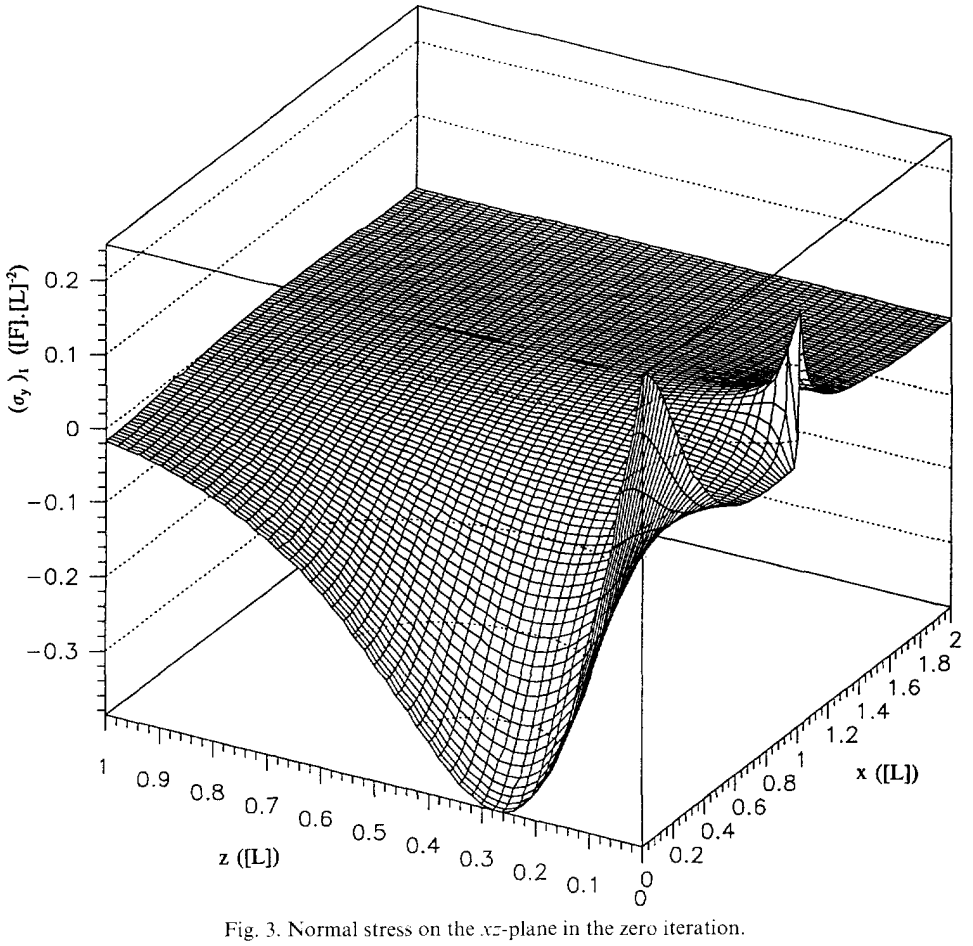

Fig. 3. Normal stress on the xz-plane in the zero iteration.

coordinates (cf. Figs 1 and B1). The K-distribution is shown in Fig. 2. The normal stresses on the xz-plane were calculated with the formulae of Appendix A and are given in Fig. 3. Expressions for the stress component $(\sigma_y)_1$ and displacement $(w)_1$ in the vicinity of the crack front are derived in Appendix B. The $(\sigma_y)_1$ stress singularity at the crack front due to the two point forces has the form [eqn (B48)]:

$$(\sigma_y)_1 \sim 2K(a, P; \rho_0, \phi_0; \nu) \frac{1}{\sqrt{\varepsilon}} \cos\frac{\theta}{2}, \quad \varepsilon \to 0, \tag{4}$$

where

$$K(a, P; \rho_0, \phi_0; \nu) \doteq 2\nu \frac{P}{\pi^2} \frac{\sqrt{a^2 - \rho_0^2}}{R^2 \sqrt{2a}} \tag{5}$$

and

$$R^2 \doteq a^2 + \rho_0^2 - 2a\rho_0 \cos\phi_0. \tag{6}$$

Note that the stress singularity disappears for $\nu = 0$. Since (cf. Figs 1 and B1):

$$\rho_0 = 0.5\,[\mathrm{L}], \quad R^2 = 1.25[\mathrm{L}]^2, \tag{7}$$

K takes the value

$$K = 0.0298\,[\mathrm{F}]/[\mathrm{L}]^{3/2}. \tag{8}$$

Here and throughout the article the following definitions are used (Bender and Orszag, 1978):

$$f(x) \sim g(x), \quad x \to x_0 \Leftrightarrow \lim_{x \to x_0} f(x)/g(x) = 1 \tag{9}$$

$$f(x) = o[g(x)], \quad x \to x_0 \Leftrightarrow \lim_{x \to x_0} f(x)/g(x) = 0 \tag{10}$$

and

$$f(x) = O[g(x)], \quad x \to x_0 \Leftrightarrow \lim_{x \to x_0} |f(x)/g(x)| < M, \tag{11}$$

for some constant M if x is sufficiently close to x_0.

The stress $(\sigma_y)_1$ at the singularity is clearly positive (tension). The crack opening near $(1, 0, 0)$ [L] amounts to [cf. Fig. B2 for the meaning of χ and ε, and eqn (B65)]

$$(w)_1 \sim 2\frac{2H(\nu, E)P}{\pi} \frac{\sqrt{\varepsilon}}{R^2} \frac{\sqrt{2a\cos\chi}\sqrt{a^2 - \rho_0^2}}{a}, \quad \varepsilon \to 0 \tag{12}$$

or

$$(w)_1 \sim 1.7208.10^{-6} \sqrt{\cos\chi}\sqrt{\varepsilon}, \quad \varepsilon \to 0, \tag{13}$$

since [cf. eqn (A33)]

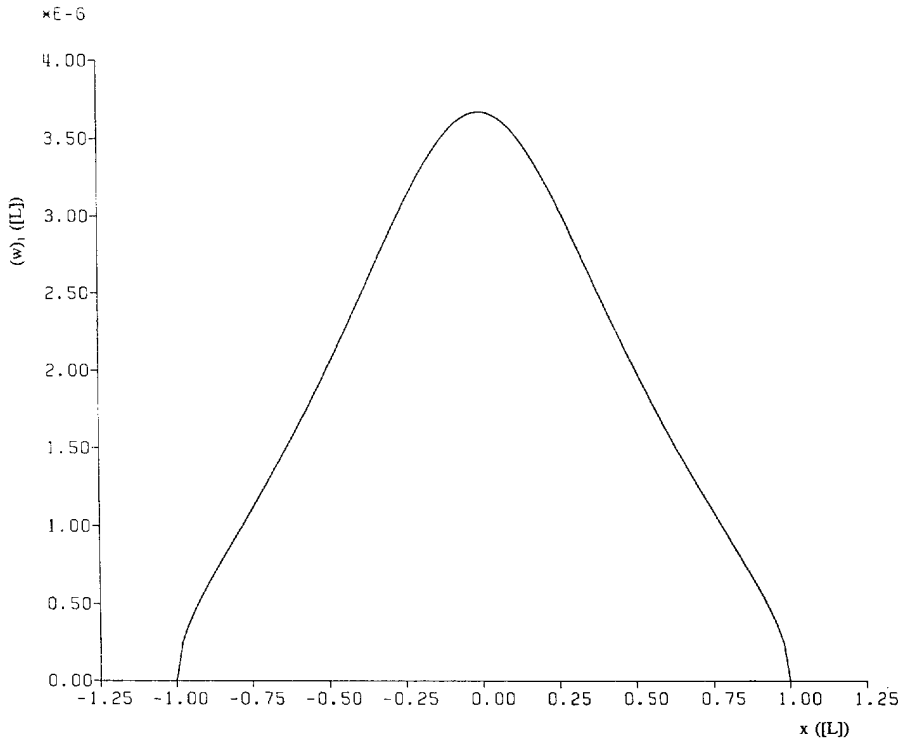

Fig. 4. Crack opening at the free surface in the zero iteration.

$$H = 1.379 \times 10^{-6}\,[\mathrm{L}]^2/[\mathrm{F}]. \tag{14}$$

The crack opening at the free boundary is shown in Fig. 4.

First iteration

Application of the inverse stress $-(\sigma_y)_1$ on the boundary of the half space $y \geqslant 0$ (Fig. 1) leads to the stresses $(\sigma_z)_2$ in Fig. 5. in the xy-plane, where

$$R_1 = \sqrt{(x-1)^2+y^2}\,[\mathrm{L}] \quad R_2 = \sqrt{(x+1)^2+y^2}\,[\mathrm{L}]. \tag{15}$$

Use was made of the formulae in Appendix C and the IMSL integration routines (IMSL, 1989; Piessens *et al.*, 1983). The stress $(\sigma_z)_2$ was calculated at approximately 1500 selected points. For values in between a Delaunay triangulation (Sloan and Houlsby, 1983) was performed followed by linear interpolation.

The stress $(\sigma_z)_2$ in the vicinity of $(1, 0, 0)$ [L] converges towards the values predicted in Appendix D [compare Fig. 6 with $f(\theta_1)$ in Fig. D2, cf. Fig. 7 for the meaning of θ_1 and r]:

$$(\sigma_z)_2 \sim 2\frac{K}{\sqrt{r}} f(\theta_1), \quad r \to 0. \tag{16}$$

It is important to notice that the application of the pressure singularity on the xz-plane at $(1, 0, 0)$ [L] leads to compressive stresses in the xy-plane.

Now the stress $-(\sigma_z)_2$ was applied to the crack faces. The stress $(\sigma_y)_3$, displacement $(w)_3$ and stress intensity factor $K(\phi)_1$ were calculated using the formulae in Appendix A. The leading behaviour of each of these quantities is calculated in Appendix E.

The stress intensity factor $K(\phi)_1$ is shown in Fig. 8. The presence of the free surface increases the K-factor everywhere except at the free surface. The increase at the deepest point is nearly 5%. The correction is zero at about 0.03 from the free surface. Figure 9

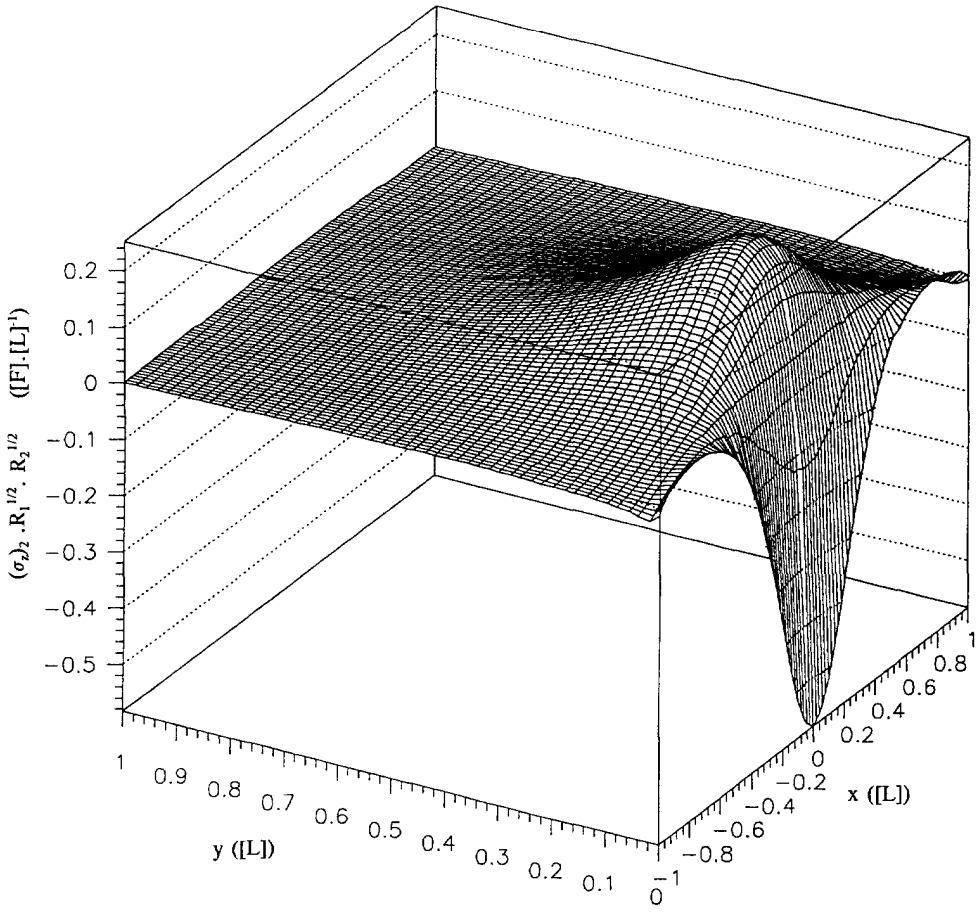

Fig. 5. Normal stress on the crack faces in the first iteration.

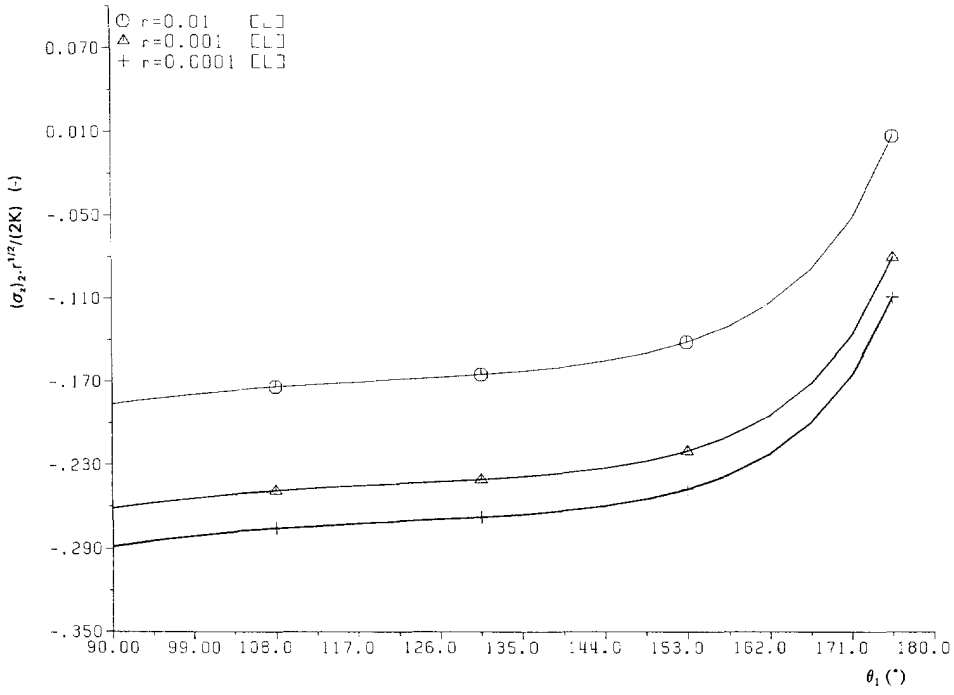

Fig. 6. Normal stress on the crack faces along a circle with radius r and centre (1,0,0) in the first iteration.

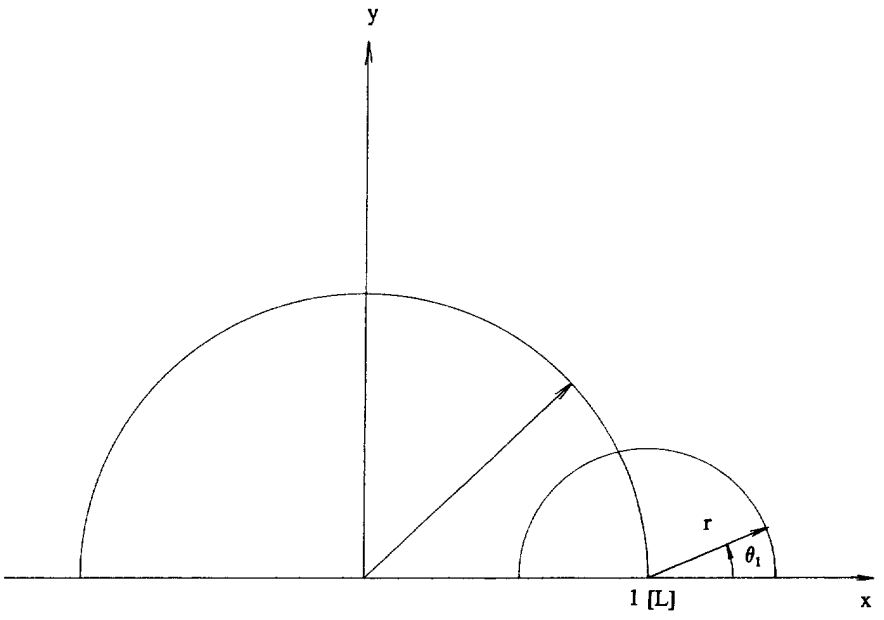

Fig. 7. Definition of the geometric parameters used in Fig. 6.

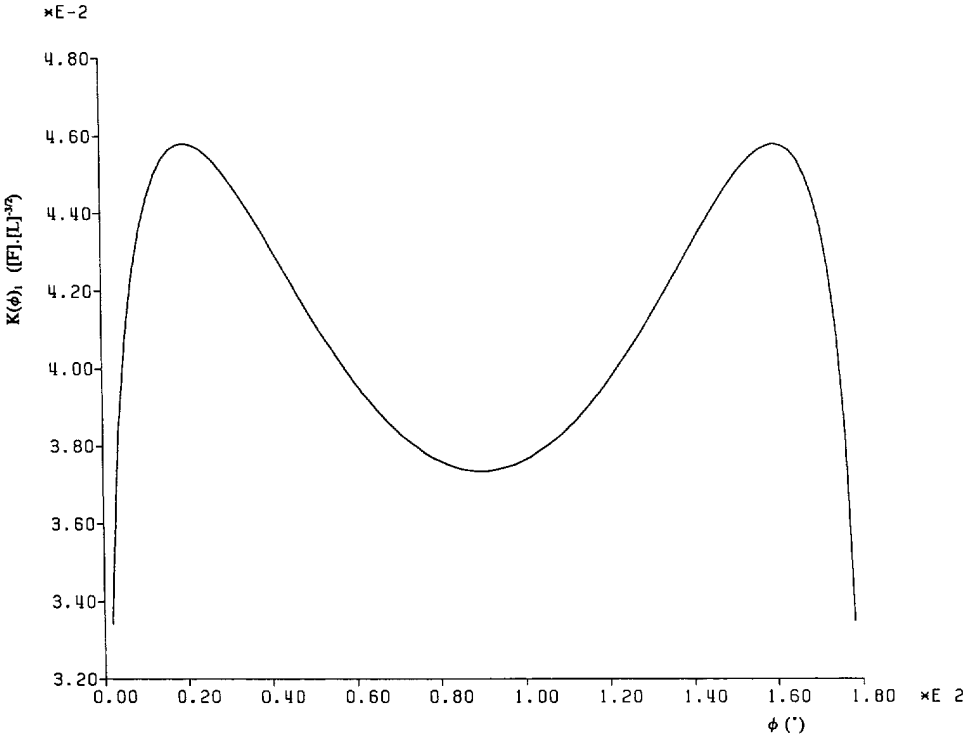

Fig. 8. Stress intensity factor distribution in the first iteration.

shows the first iteration values close to the free surface. The leading behaviour takes the form (cf. Appendix E):

$$K(\phi)_1 = 2\frac{2\sqrt{2}}{\pi\sqrt{\pi}} K(a, P; \rho_0, \phi_0; \nu) F(\nu) \ln \phi + O(1), \quad \phi \to 0, \tag{17}$$

where $F(\nu) = 0.1788 + 0.3856\ \nu$. This is confirmed by the numerical data in Fig. 9, since

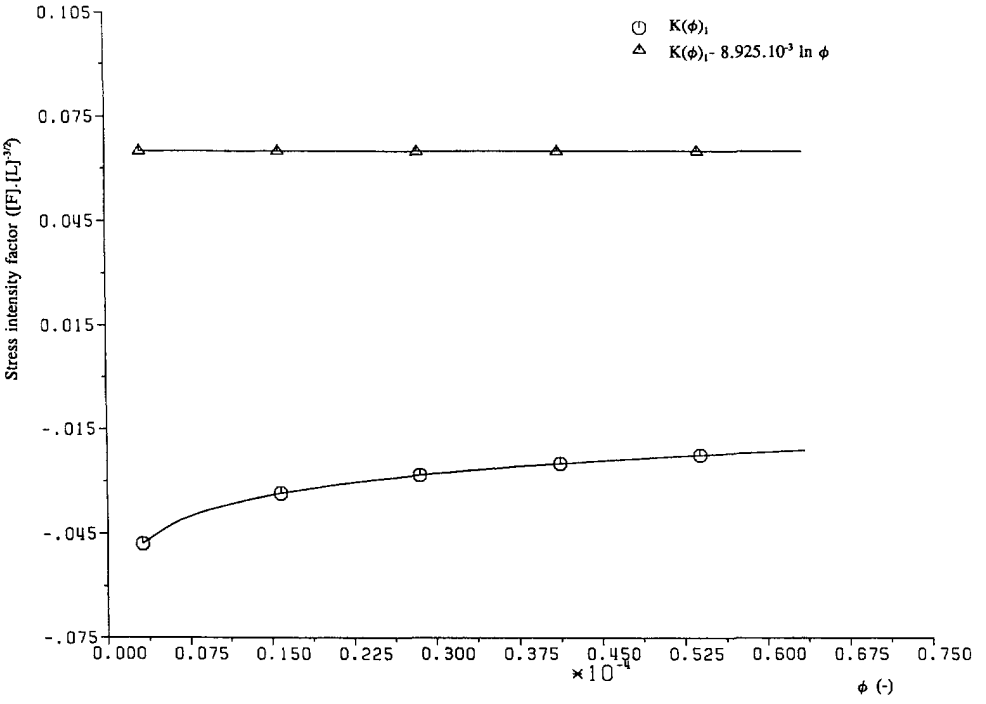

Fig. 9. K-distribution in the first iteration close to the free surface.

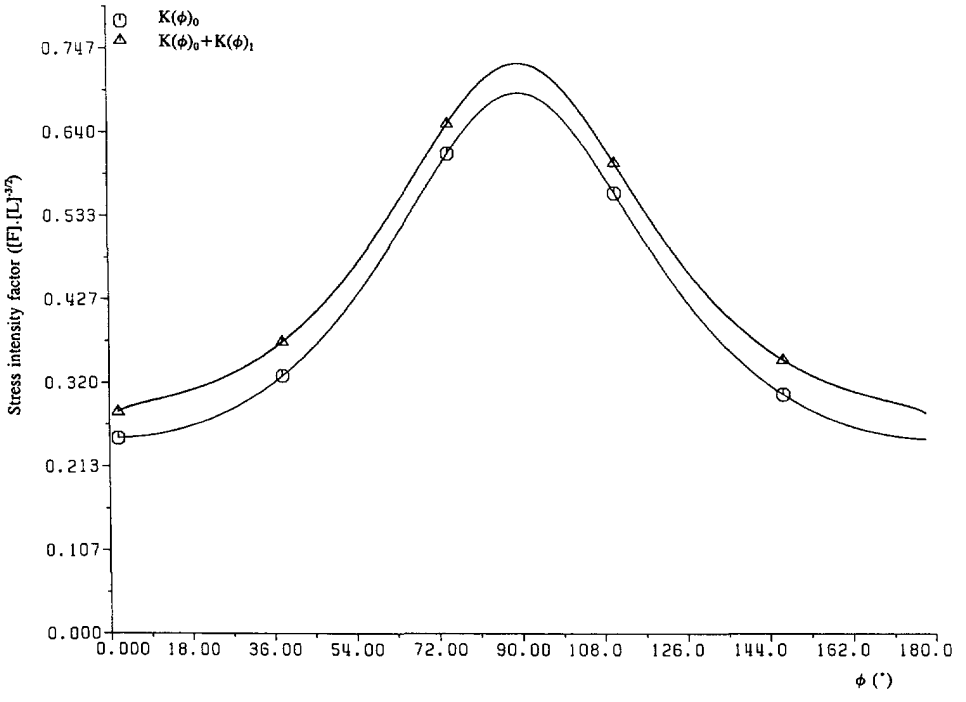

Fig. 10. Sum of the zero and first iteration values of the K-distribution.

subtraction of the leading behaviour in eqn (17) from $K(\phi)_1$ yields a constant. The sum of the zero and first iterations is depicted in Fig. 10.

The stress $(\sigma_y)_3$ (Fig. 11) has decreased in magnitude compared to $(\sigma_y)_1$ except in a small layer at the free surface. The value at $z = 0$ is actually extrapolated from $z = 0.001$. The leading behaviour near $(1, 0, 0)$ [L] has the form (ε and θ are explained in Fig. E1)

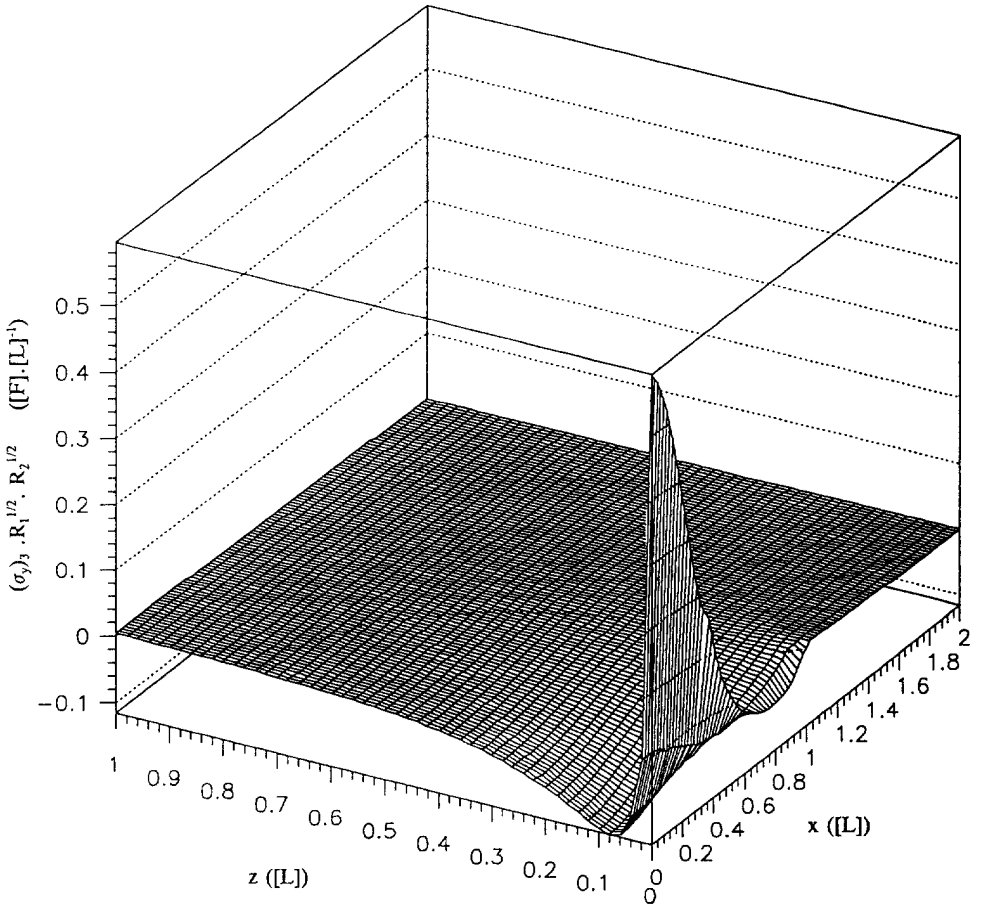

Fig. 11. Normal stress on the free surface in the first iteration.

$$(\sigma_{\gamma})_3 = 2\frac{4\nu}{\pi^2} K(a, P; \rho_0, \phi_0; \nu) \cos\frac{\theta}{2} F(\nu) \frac{\ln \varepsilon}{\sqrt{\varepsilon}} + O\left(\frac{1}{\sqrt{\varepsilon}}\right), \quad \varepsilon \to 0. \tag{18}$$

The first correction for the crack opening $(w)_3$ is generally positive (Fig. 12). Figure 13 shows the new total crack opening. However, the leading behaviour near (1, 0, 0) [L]:

$$(w)_3 = 2\frac{8}{\pi} H(\nu, E) K(a, P; \rho_0, \phi_0; \nu) \sqrt{\cos\chi}\, F(\nu) \sqrt{\varepsilon} \ln(\varepsilon) + O(\sqrt{\varepsilon}), \quad \varepsilon \to 0 \tag{19}$$

$$= 0.6167 \times 10^{-7} \sqrt{\varepsilon} \ln \varepsilon \sqrt{\cos\chi} + O(\sqrt{\varepsilon}), \quad \varepsilon \to 0 \tag{20}$$

(see Fig. B2 for the meaning of χ) which can be complemented by means of the numerical data in Fig. 14 to

$$(w)_3 \sim 0.6167 \times 10^{-7} \sqrt{\varepsilon} \ln(\varepsilon) \sqrt{\cos\chi} + 0.5207 \times 10^{-6} g(\chi) \sqrt{\varepsilon}, \quad \varepsilon \to 0, \tag{21}$$

where $0 \leqslant g(\chi) \leqslant 1$ (Fig. 15), shows that $(w)_3$ will be negative for very small ε values. Solving $(w)_1 + (w)_3 = 0$ [cf. eqns (13) and (21)] yields an estimate of the pressure zone:

$$\varepsilon_{\text{pres}}(\chi) = \exp\left[\frac{-1.7208 \times 10^{-6} \sqrt{\cos\chi} - 0.5207 \times 10^{-6} g(\chi)}{0.6167 \times 10^{-7} \sqrt{\cos\chi}}\right]. \tag{22}$$

The values of $\varepsilon_{\text{pres}}$ are of the order of magnitude of 10^{-16} [L] (Fig. 16). Due to this crack

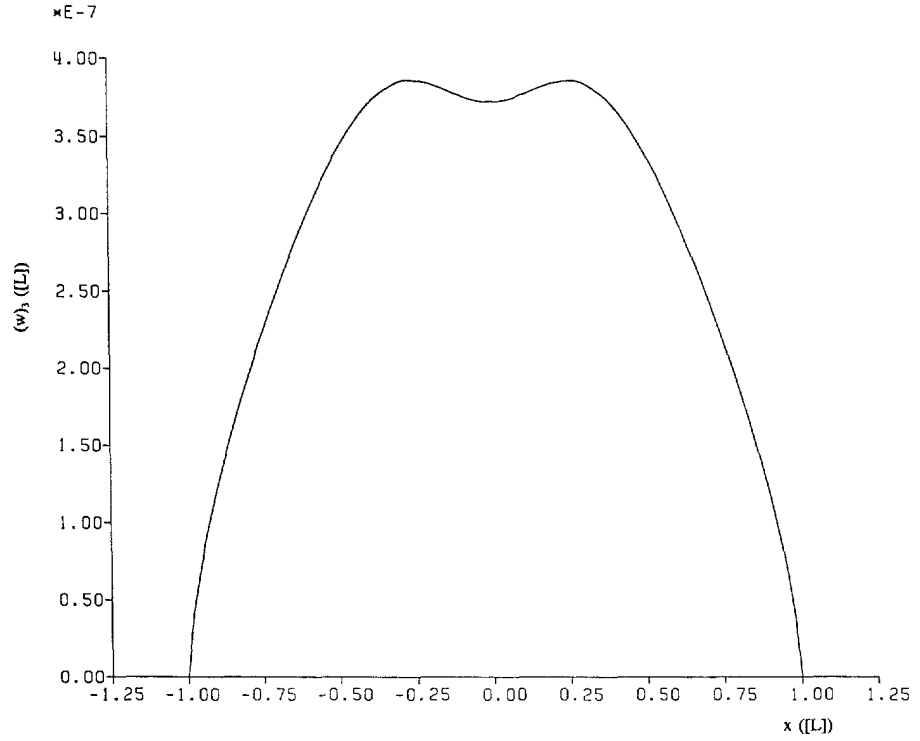

Fig. 12. Crack opening at the free surface in the first iteration.

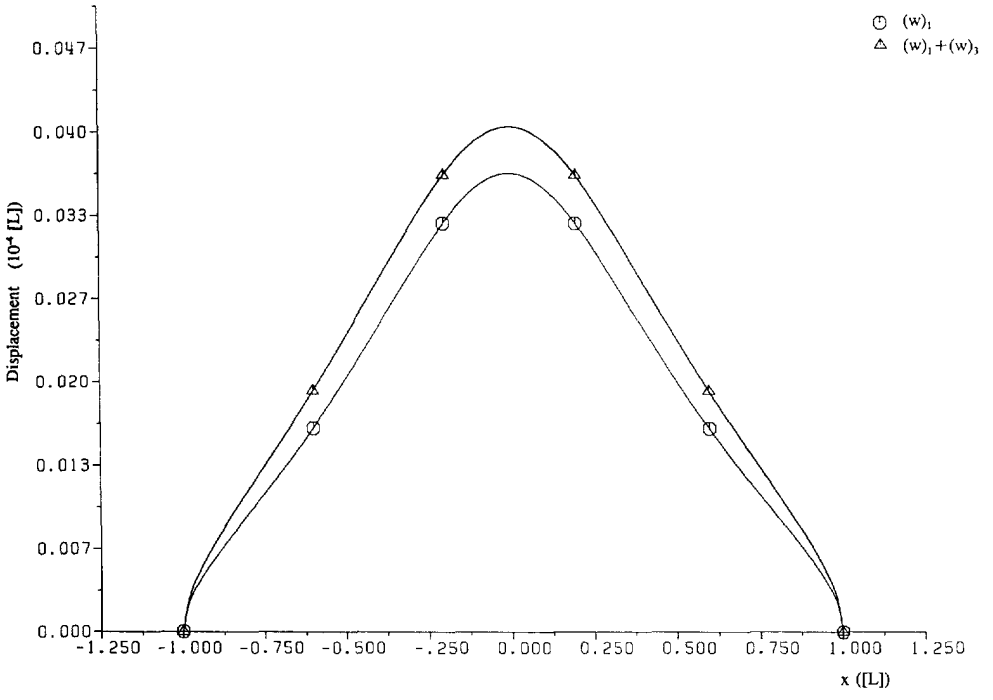

Fig. 13. Sum of the zero and first iteration values of the crack opening at the free surface.

closure the problem is actually non-linear. The stress $(\sigma_z)_2'$ inside the pressure zone which is needed to close the crack will be smaller than $(\sigma_z)_2$:

$$(\sigma_z)_2' = (\sigma_z)_2 \, h(\varepsilon, \chi), \quad \varepsilon \leqslant \varepsilon_{\text{pres}}(\chi), \quad 0 \leqslant h(\varepsilon, \chi) \leqslant 1, \tag{23}$$

whereas

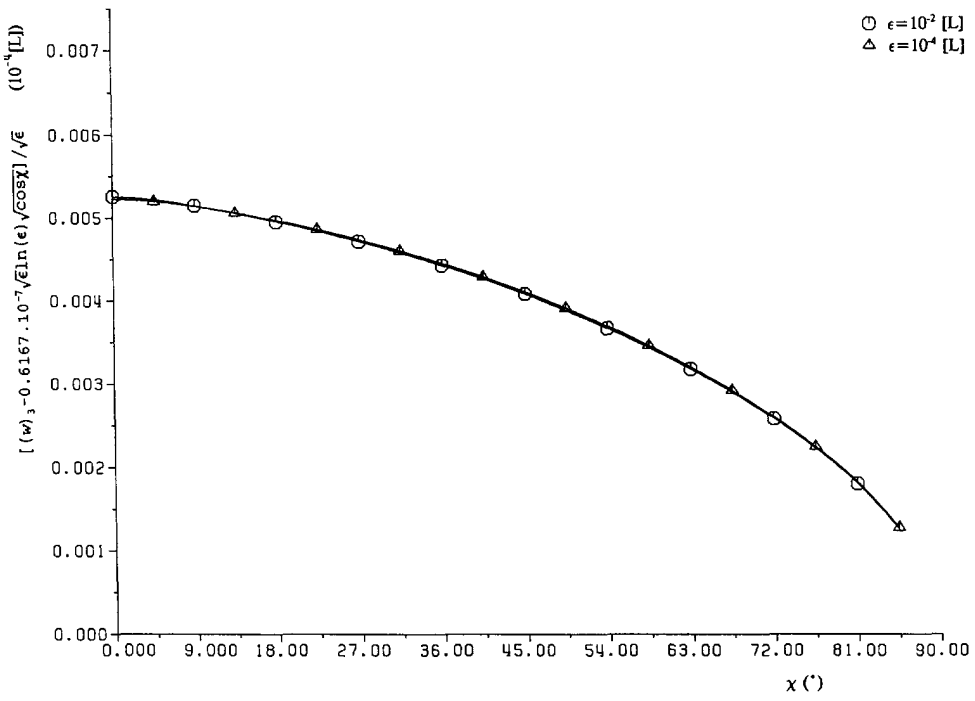

Fig. 14. Coefficient of the second term in the asymptotic expansion of the crack opening at the free surface in the first iteration.

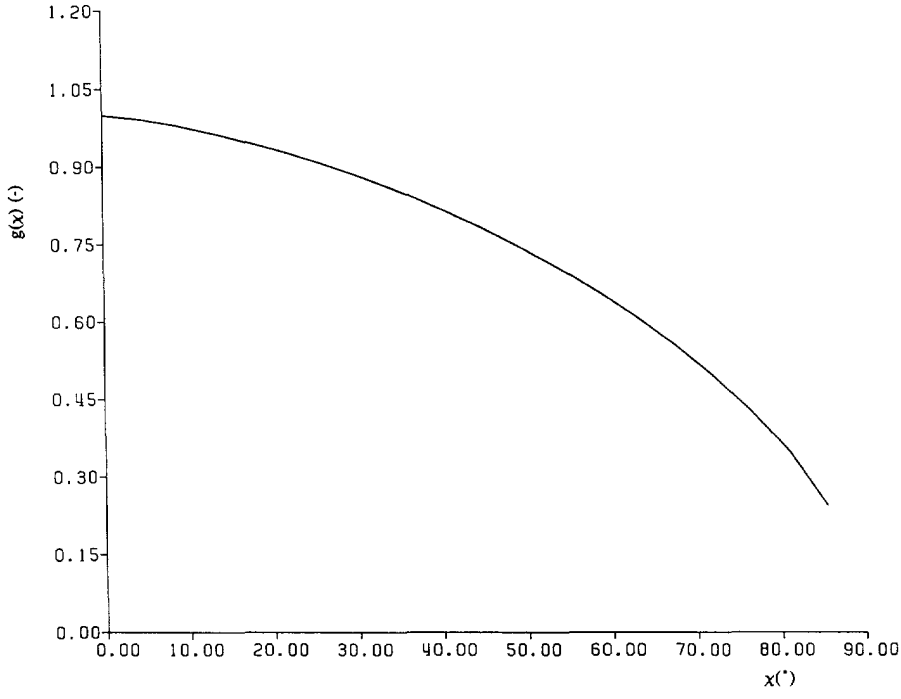

Fig. 15. Normalized coefficient function g.

$$(\sigma_z)'_2 = (\sigma_z)_2\,, \quad \varepsilon > \varepsilon_{\text{pres}}(\chi). \tag{24}$$

Furthermore, $(w)'_3$ due to $(\sigma_z)'_2$ must satisfy

$$(w)'_3 + (w)_1 = 0\,, \quad \varepsilon \leqslant \varepsilon_{\text{pres}}(\chi) \tag{25}$$

$$(w)'_3 + (w)_1 > 0\,, \quad \varepsilon > \varepsilon_{\text{pres}}(\chi). \tag{26}$$

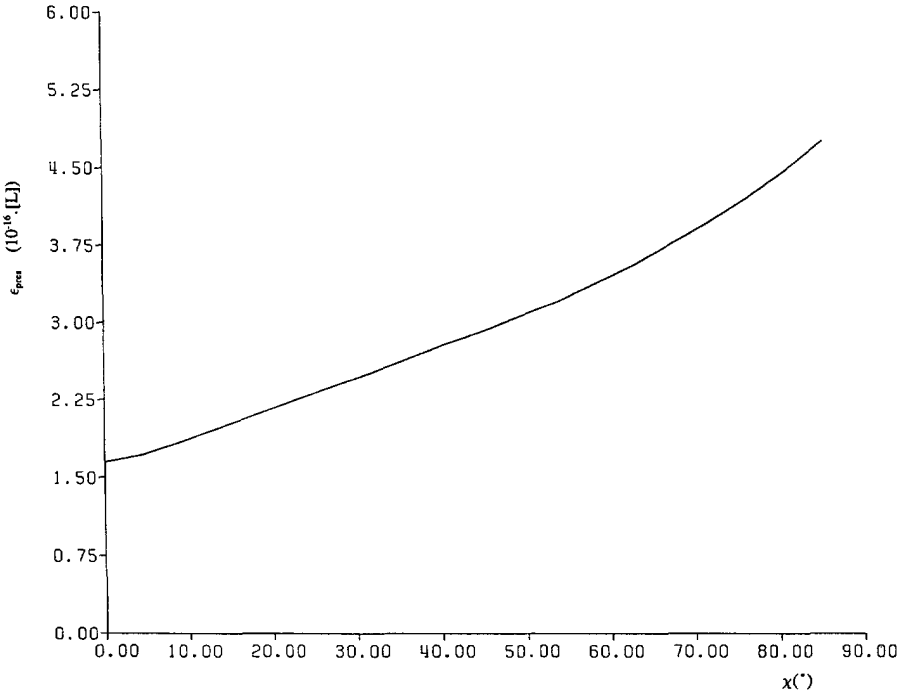

Fig. 16. Estimate of the size of the pressure zone.

Here this non-linear problem will not be solved. However, in Appendix E it is proven that for $\varepsilon > \varepsilon_{\text{pres}}(\chi)$ the leading behaviour in eqns (18) and (19) is not influenced. Since $\varepsilon_{\text{pres}}$ is very small the pressure zone does not appear in the numerical calculations.

It is very interesting to notice that the boundary of the pressure zone coincides with $K(\phi)_0 + K(\phi)_1 = 0$. Indeed, $K(\phi)_0$ satisfies [cf. eqn (B75)]:

$$K(\phi)_0 \sim K(a, P; \rho_0, \phi_0; \nu)\frac{\sqrt{2\pi}}{\nu} \sim 0.2490, \quad \phi \to 0 \tag{27}$$

and taking eqn (17) for $K(\phi)_1$ together with the numerical data of Fig. 9:

$$K(\phi)_1 \sim \frac{4\sqrt{2}}{\pi\sqrt{\pi}} K(a, P; \rho_0, \phi_0; \nu) F(\nu) \ln \phi + C_0(a, P; \rho_0, \phi_0; \nu), \quad \phi \to 0$$

$$\sim 0.0089247 \ln \phi + 0.066, \quad \phi \to 0, \tag{28}$$

one obtains $K(\phi)_0 + K(\phi)_1 = 0$ for $\phi = 4.7 \times 10^{-16}$. This agrees with the value of $\varepsilon_{\text{pres}}$ for $\chi = 90°$ in Fig. 16.

Dropping the second term in eqn (21) or eqn (28) one finds in both cases the following analytical expression for a first rough estimate of $\varepsilon_{\text{pres}}$:

$$\varepsilon_{\text{pres}} \simeq \exp\left[-\frac{\pi^2}{4\nu F(\nu)}\right], \tag{29}$$

which yields $\varepsilon_{\text{pres}} = 7.6 \times 10^{-13}$ [L], independent of the location of P (ρ_0 and ϕ_0)! Since it is generally quite tedious to find the second terms in eqns (21) or (28), eqn (29) is useful as a first approximation. It shows that $\varepsilon_{\text{pres}}$ is indeed very small independent of the location of P, provided that $a\phi \ll R$ [cf. the domain of validity of eqn (B75)]. Taking the second term of eqn (21) or (28) into account decreases $\varepsilon_{\text{pres}}$ even further.

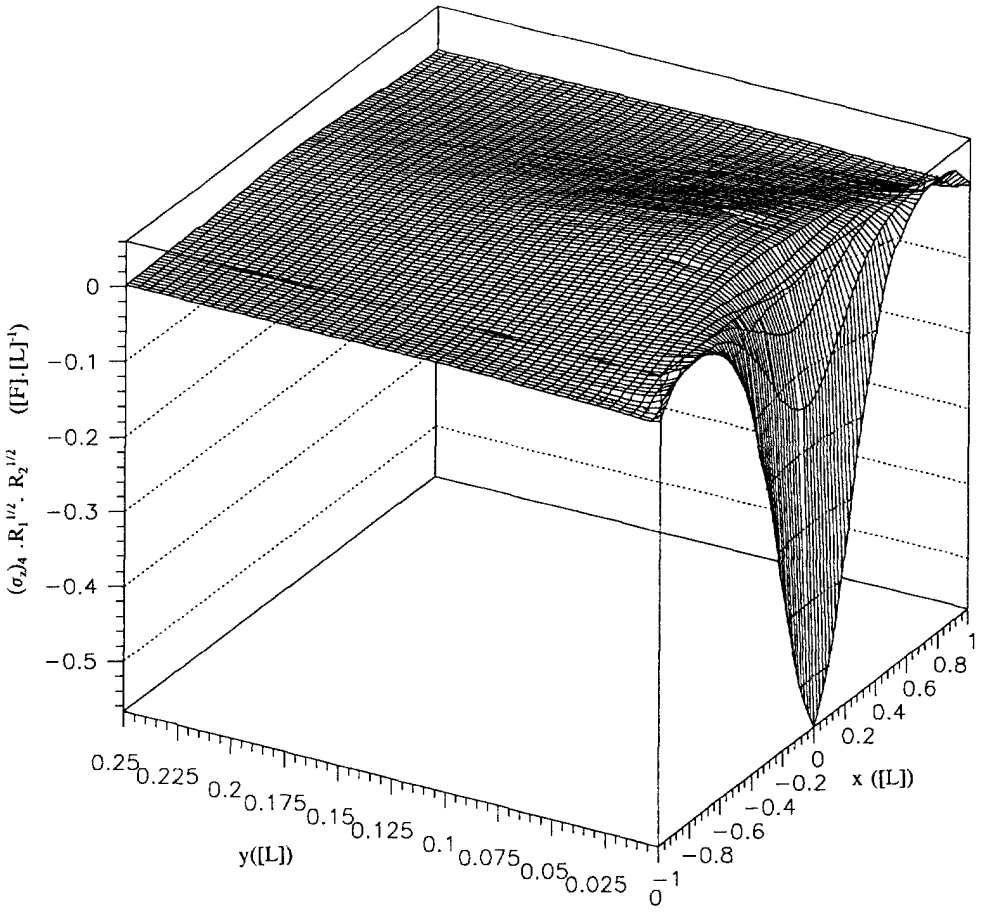

Fig. 17. Normal stress on the free surface in the second iteration.

Second iteration

Application of the inverse stress $-(\sigma_y)_3$ on the boundary of the half space $y \geqslant 0$ leads to the stresses $(\sigma_z)_4$ in Fig. 17 in the xy-plane. Comparing these stresses with $(\sigma_z)_2$ in Fig. 5, there is an overall decrease in magnitude of the stress values except for the small peak near $y = 0$. In Appendix F it is shown that for $\varepsilon_{\text{pres}}{}^{1/k} \ll \varepsilon \ll 1, k > 1$, where ε is the distance from $(1, 0, 0)$ [L] in the xy-plane, the leading behaviour of $(\sigma_z)_4$ satisfies

$$(\sigma_z)_4 = O\left(\frac{\ln \varepsilon}{\sqrt{\varepsilon}}\right), \quad \varepsilon \to 0. \tag{30}$$

Application of the inverse stresses leads to the K-distribution $K(\phi)_2$ in Fig. 18. Adding this second correction to the previous ones, Fig. 19 is obtained. The K-distribution seems to converge smoothly. Regarding $K(\phi)_1 + K(\phi)_2$ (Fig. 20), it is observed that the second correction moves the maximum of the first correction towards the free surface.

4. DISCUSSION OF THE K-DISTRIBUTION NEAR THE FREE SURFACE

The results of the previous section show that, due to the presence of the free surface, the K-values have generally increased. This increase is smallest at the deepest point of the crack (about 5% in the example) and increases towards the free surface. However, at the free surface the stress intensity factor decreases sharply towards zero. The negative values obtained in the first iteration point to the existence of a small pressure zone at the intersection of the crack with the free surface. A first estimate reveals that the size of this zone is extremely small (10^{-16} [L]). This result must be viewed in the context of a linear elastic

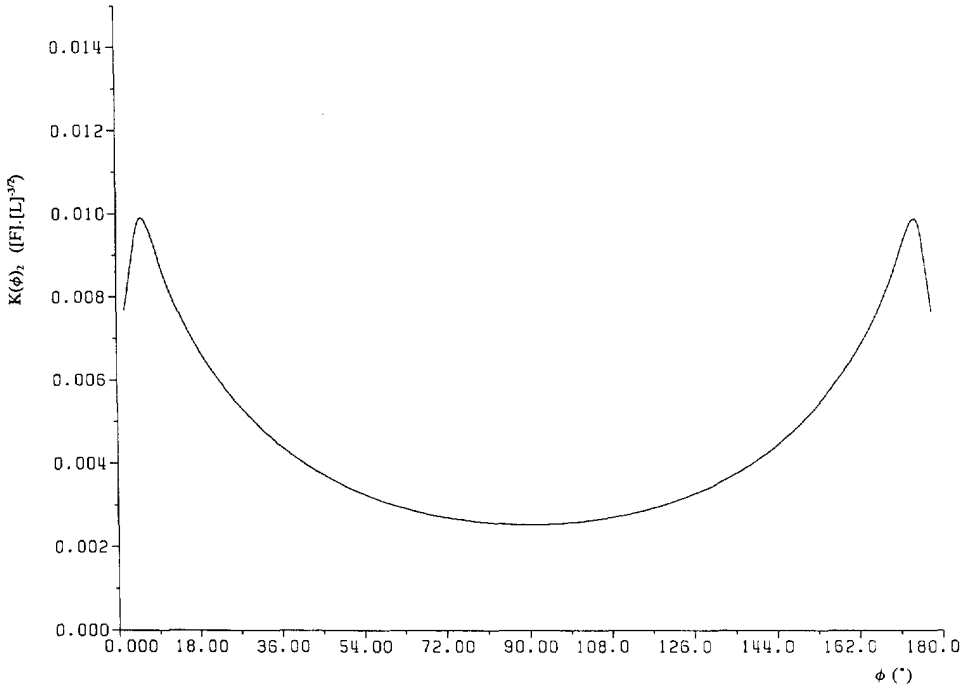

Fig. 18. *K*-distribution in the second iteration.

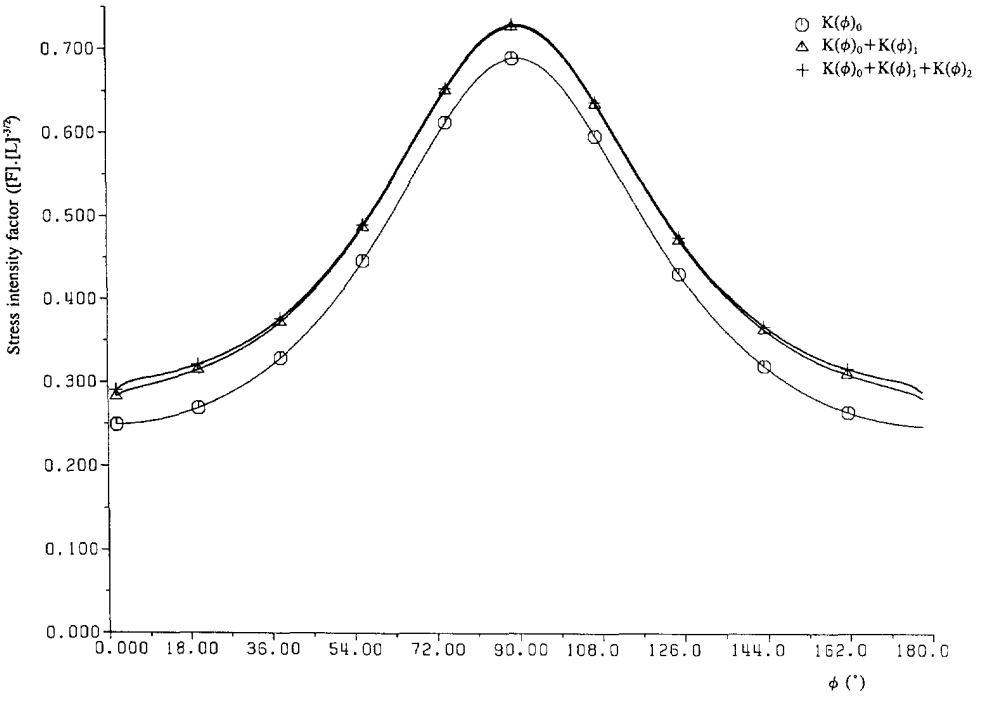

Fig. 19. Sum of the zero, first and second order iteration values of the *K*-distribution.

homogeneous and isotropic material and is as such acceptable. No assumption was made about an atomic structure.

The decreasing *K*-values at the free surface are in agreement with observations that the propagation of half circular surface cracks frequently slows down at the free surface. Furthermore, recent numerical work suggests a decrease of the stress singularity at the free surface from the generic $r^{-0.5}$ to about r^{λ}, $\lambda > -0.5$ (Becker, 1989). This leads to a zero stress intensity factor at the free surface.

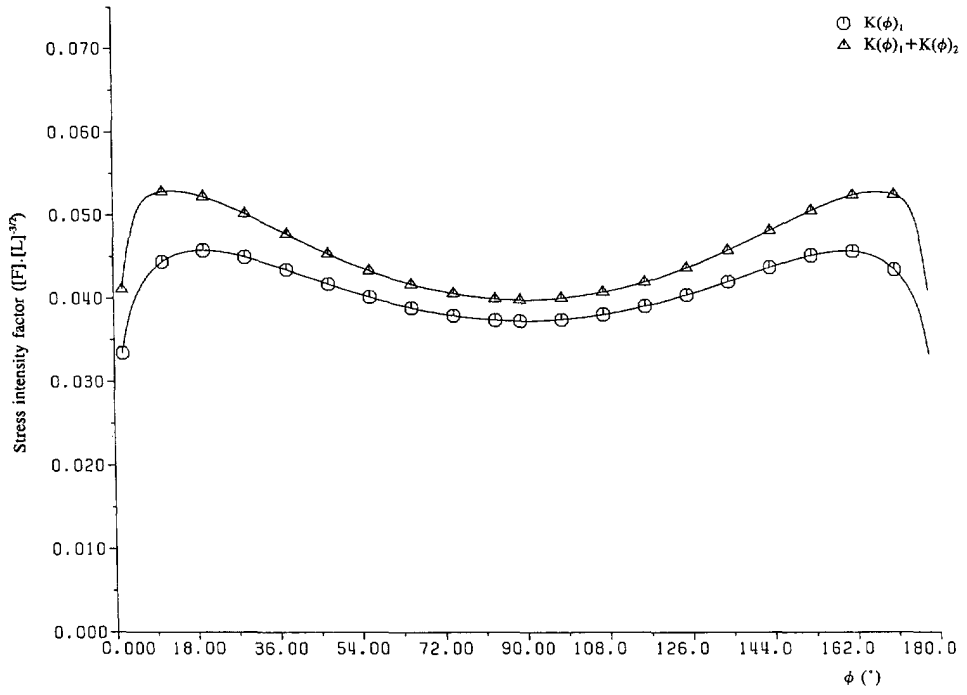

Fig. 20. Sum of the first and second iteration values of the K-distribution.

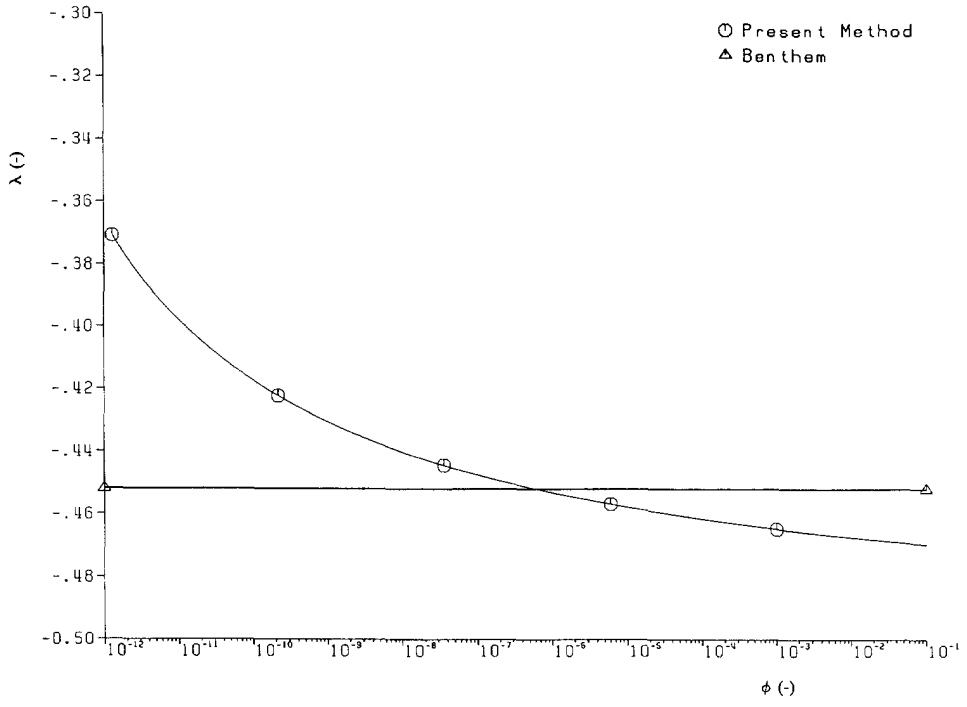

Fig. 21. λ-values near the free boundary.

Whereas most recent numerical work points towards a zero stress intensity factor at the free surface, the way in which the K-factor tends to this zero value is equivocal. Benthem, who did a substantial amount of work on the subject, assumed a $r^{\lambda}f(\theta, \varphi)$ stress solution where r, θ and φ are spherical coordinates with the origin located at the intersection of the crack with the free surface. Using an eigenfunction expansion technique, he obtained for $\nu = 0.3$ an $r^{-0.45}$ stress singularity and consequently an $r^{0.05}$ behaviour for the stress intensity factor (Benthem, 1977). Similar results were obtained using finite differences (Benthem,

1980). Becker, on the other hand, using the same assumption but a different numerical technique (the finite element method) obtained an $r^{-0.40}$ stress singularity (Becker, 1989).

Due to the occurrence of the pressure zone and the resulting non-linear problem, the present theory cannot give an ultimate answer to this question. However, it is very interesting to analyse the asymptotic behaviour of the present K-solution near the free surface using an r^{λ} assumption for the stress and consequently an $r^{\lambda+0.5}$ solution for K. Equating $Cr^{\lambda+0.5}$, or equivalently $C\phi^{\lambda+0.5}$ ($a = 1$ [L]), where C is a constant, to $K(\phi)_0 + K(\phi)_1$ [eqns (27) and (28)] yields for the point load position investigated in the previous section:

$$\frac{(0.0089 \ln(\phi) + 0.3148)}{\sqrt{\phi}} = C\phi^{\lambda} \tag{31}$$

or

$$\lambda = \frac{\mathrm{d}}{\mathrm{d}(\log \phi)}\left[\log\left(\frac{0.0089 \ln \phi + 0.3148}{\sqrt{\phi}}\right)\right]. \tag{32}$$

This function is represented in Fig. 21, together with the λ-value obtained by Benthem. The curves clearly do not coincide. However, they intersect and are generally of the same order of magnitude. Furthermore, notice that the λ-value arrived at by the present method needs about eight orders of magnitude to change from -0.47 to -0.43, i.e. the function is virtually constant over a large range. This also implies that, if there really is a logarithmic singularity involved, it would be very difficult to detect this either by finite differences or experimental techniques [e.g. Smith (1988)], since ϕ-values as small as $\phi = 10^{-9}$ yield λ-values which are altogether not that different from the λ-value for say $\phi = 10^{-3}$.

Finally, it is worthwhile pointing out that due to the disappearance of the σ_y stress singularity at the crack front for $\nu = 0$, the logarithmic term in $K(\phi)_1$, and consequently the boundary layer near the free boundary, vanishes for this value of ν. This is in agreement with the findings of Benthem.

5. GREEN FUNCTIONS FOR A REPRESENTATIVE SET OF POINT LOAD POSITIONS

Section 3 of this article treated one specific position of the point load. It would clearly be very useful to have the complete K-distribution for a series of representative positions of the point load. This would allow for the calculation of the K-distribution due to arbitrary loading on the crack faces. To this end, a matrix of about 60 representative point load positions has been composed and the corresponding zero and first iteration K-distributions $K(\phi)_0$ and $K(\phi)_1$ were calculated. Due to the symmetry of the problem only point load positions within a quarter circular crack in the positive x–y quadrant have been considered. The matrix consisted of a relatively uniform distribution over the complete quarter circle (Fig. 22), completed by a detailed analysis of the region near the free boundary (Fig. 23) with a couple of additional points in the area close to the intersection of the crack front with the free boundary (Fig. 24).

Again, $a = 1$ [L] and $P = 1$ [F] were assumed. This is not really a restriction since the units of length and force can be chosen arbitrarily. However, the formulae in Section 3 have illustrated that the results are a function of Poisson's coefficient, ν. Here $\nu = 0.3$ was taken, and consequently the numerical results only apply to this (in practice frequently used) ν-value.

For simplicity the point load positions were identified with a code consisting of two characters. For the point loads in Fig. 22 the characters actually reduce to two integer numbers $0 \leqslant i, j \leqslant 9$ forming a two digit number ij and uniquely defining ρ_0 and ϕ_0 by

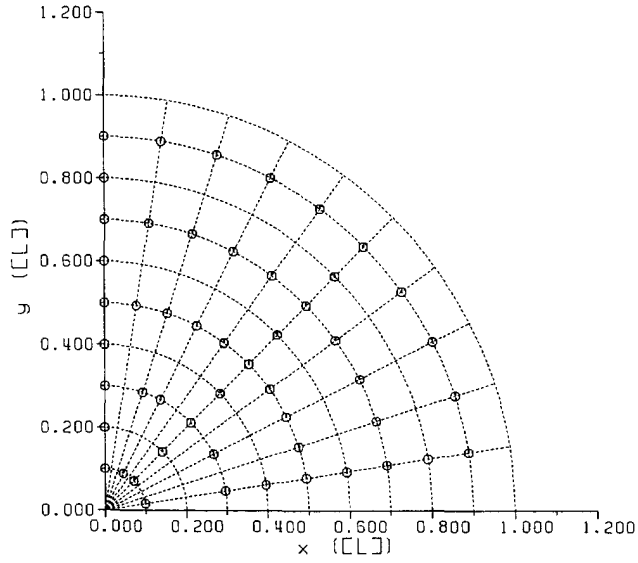

Fig. 22. Matrix of evenly distributed point load positions.

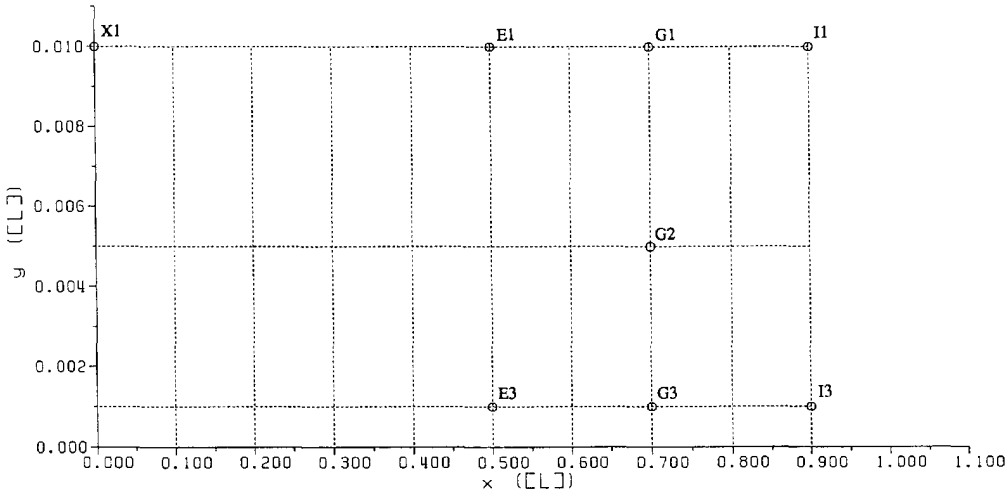

Fig. 23. Point load positions near the free surface.

$$\rho_0 = 0.1\, i\,[\mathrm{L}] \tag{33}$$

$$\phi_0 = \frac{\pi}{20}(10-j). \tag{34}$$

The code for the other point load positions is illustrated in Figs 23 and 24. The code for all point loads together with the numerical values for ρ_0 and ϕ_0 is given in Table 1. For the zero iteration of the K-distribution, $K(\phi)_0$, an analytical expression exists [eqns (2) and (3)].

For the first iteration distribution $K(\phi)_1$ no analytical expression exists, but the asymptotic behaviour near the free boundary ($\phi = 0, \pi$) is known [eqn (28)]. For $\phi \to 0$ one can write

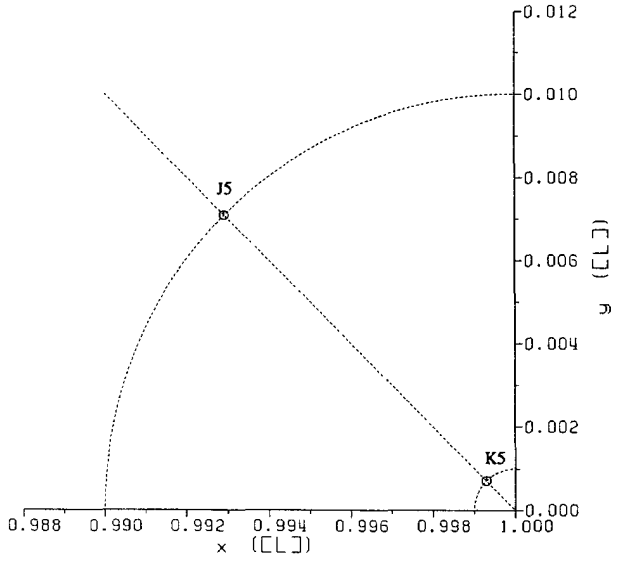

Fig. 24. Point load positions near the intersection of the crack front with the free surface.

$$K(\phi)_I \sim 2\frac{2\sqrt{2}}{\pi\sqrt{\pi}}K(a,P;\rho_0,\phi_0;\nu)F(\nu)\ln\phi + C_0(a,P;\rho_0,\phi_0;\nu), \quad \phi \to 0 \tag{35}$$

$$\sim \left(\frac{2}{\pi}\right)^{7/2}\frac{\nu F(\nu)\sqrt{a^2-\rho_0^2}}{(a^2+\rho_0^2-2a\rho_0\cos\phi_0)\sqrt{2a}}\ln\phi + C_0(a,P;\rho_0,\phi_0;\nu), \quad \phi \to 0 \tag{36}$$

and for $\phi \to \pi$

$$K(\phi)_I \sim 2\frac{2\sqrt{2}}{\pi\sqrt{\pi}}K(a,P;\rho_0,\pi-\phi_0,\nu)F(\nu)\ln(\pi-\phi) + C_\pi(a,P;\rho_0,\phi_0;\nu), \quad \phi \to \pi \tag{37}$$

$$\sim \left(\frac{2}{\pi}\right)^{7/2}\frac{\nu F(\nu)\sqrt{a^2-\rho_0^2}}{(a^2+\rho_0^2+2a\rho_0\cos\phi_0)\sqrt{2a}}\ln(\pi-\phi) + C_\pi(a,P;\rho_0,\phi_0;\nu), \quad \phi \to \pi. \tag{38}$$

Both asymptotic behaviours can be amalgamated in the form:

$$K(\phi)_I \sim \left(\frac{2}{\pi}\right)^{7/2}\frac{\nu F(\nu)\sqrt{a^2-\rho_0^2}}{(a^2+\rho_0^2-2a\rho_0\cos\phi_0\cos\phi)\sqrt{2a}}\ln(\sin(\phi)) + \left[C_0 + \frac{C_\pi - C_0}{\pi}\phi\right],$$

$$\phi \to 0,\pi; \quad 0 < \phi < \pi. \tag{39}$$

For all point load positions $K(\phi)_I$ was calculated numerically (following the approach of Section 3) and in all cases the solution satisfied relation (39). For the sake of brevity the function on the right of relation (39) (the complete expression after the $\sim$ symbol) will be called $K_a(\phi)_I$. The calculated values of C_0 and C_π are given in Table 1. In Fig. 25 iso-lines of constant C_0 are drawn in steps of 0.1 [F] $[L]^{-3/2}$. This shows that C_0 strongly increases towards the intersection of the crack front and the free surface at $\phi = 0$, and probably exhibits a singularity there.

In order to make the numerical values of $K(\phi)_I$ generally available, the asymptotic behaviour $K_a(\phi)_I$ has been subtracted and the resulting function was modelled by means of B-splines. To this end, the IMSL subroutine DBSVLS was used (computes the variable knot B-spline least squares approximation to given data). The resulting B-splines are characterized by two integers KORDER and NCOEF, a real vector BSCOEF of length

Table 1. Point load positions and values for C_0 and C_π

	$\phi_0(-)$	ρ_0 ([L])	C_0 ([F]/[L]$^{-3/2}$)	C_π
10	1.57080	0.10000	0.16836	0.16836
13	1.09956	0.10000	0.18540	0.15761
15	0.78540	0.10000	0.19860	0.15360
19	0.15708	0.10000	0.16986	0.11867
20	1.57080	0.20000	0.14131	0.14130
25	0.78540	0.20000	0.20210	0.12450
30	1.57080	0.30000	0.11320	0.11321
32	1.25664	0.30000	0.13334	0.10281
33	1.09956	0.30000	0.14866	0.10018
35	0.78540	0.30000	0.19330	0.09889
37	0.47124	0.30000	0.25884	0.10189
39	0.15708	0.30000	0.33028	0.10669
40	1.57080	0.40000	0.08757	0.08757
45	0.78540	0.40000	0.17350	0.07791
49	0.15708	0.40000	0.40835	0.08915
50	1.57080	0.50000	0.06552	0.06553
51	1.41372	0.50000	0.07114	0.06200
52	1.25664	0.50000	0.07976	0.06005
53	1.09956	0.50000	0.09284	0.05930
54	0.94248	0.50000	0.11284	0.05956
55	0.78540	0.50000	0.14370	0.06075
56	0.62832	0.50000	0.19195	0.06281
57	0.47124	0.50000	0.26628	0.06569
58	0.31416	0.50000	0.37421	0.06935
59	0.15708	0.50000	0.50901	0.07355
60	1.57080	0.60000	0.04733	0.04732
65	0.78540	0.60000	0.10720	0.04675
69	0.15708	0.60000	0.62983	0.05893
70	1.57080	0.70000	0.03266	0.03266
71	1.41372	0.70000	0.03423	0.03197
72	1.25664	0.70000	0.03718	0.03193
73	1.09956	0.70000	0.04243	0.03247
74	0.94248	0.70000	0.05172	0.03350
75	0.78540	0.70000	0.06904	0.03502
76	0.62832	0.70000	0.10396	0.03707
77	0.47124	0.70000	0.18060	0.03966
78	0.31416	0.70000	0.36667	0.04290
79	0.15708	0.70000	0.79100	0.04650
80	1.57080	0.80000	0.02098	0.02098
85	0.78540	0.80000	0.03548	0.02493
89	0.15708	0.8000	0.90884	0.03478
90	1.57080	0.90000	0.01154	0.01154
91	1.41372	0.90000	0.01107	0.01208
92	1.25664	0.90000	0.01071	0.01276
93	1.09956	0.90000	0.01049	0.01350
94	0.94248	0.90000	0.01059	0.01439
95	0.78540	0.90000	0.01142	0.01546
96	0.62832	0.90000	0.01473	0.01673
97	0.47124	0.90000	0.02739	0.01828
98	0.31416	0.90000	0.09080	0.02015
99	0.15708	0.90000	0.63625	0.02239
X1	1.57080	0.01000	0.07400	0.07402
E1	0.02000	0.50000	0.59329	0.07379
E3	0.00200	0.50000	0.50423	0.06306
G1	0.01429	0.70000	1.35498	0.05032
G2	0.00714	0.70000	1.34179	0.04978
G3	0.00143	0.70000	1.24861	0.04683
I1	0.01111	0.90000	7.37859	0.02500
I3	0.00111	0.90000	5.67178	0.02156
J5	0.00712	0.99295	88.67998	0.00555
K5	0.00071	0.99929	4736.64000	0.00406

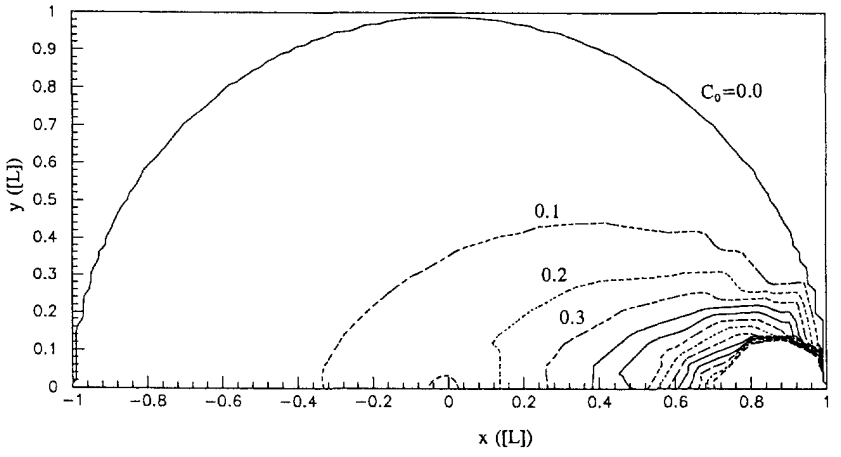

Fig. 25. Lines of constant C_0.

Table 2. BSCOEF (NCOEF = 6)

	BSCOEF (1)	BSCOEF (2)	BSCOEF (3)	BSCOEF (4)	BSCOEF (5)	BSCOEF (6)
J5	1982.01	−68.85	−88.09	−56.56	−26.59	2.82
K5	183366.89	−11419.22	−4738.60	−3060.66	−1453.75	150.60

Table 3. XKNOT and error values (NCOEF = 6)

	XKNOT (4)	XKNOT (5)	XKNOT (6)	XKNOT (7)	Error (%)
J5	−0.100	0.051	0.118	3.242	0.121
K5	−0.100	0.047	0.048	3.242	0.029

NCOEF and a real vector XKNOT of length NCOEF + KORDER for which the following relations apply:

$$\text{XKNOT}(i) = \text{XKNOT}(\text{KORDER}), i = 1, 2, \ldots, \text{KORDER} - 1 \tag{40}$$

$$\text{XKNOT}(i) = \text{XKNOT}(\text{NCOEF} + 1), i = \text{NCOEF} + 2, \ldots, \text{NCOEF} + \text{KORDER}. \tag{41}$$

Tables 2–9 give the values of BSCOEF and XKNOT for all selected point force locations. For all point loads KORDER = 4 was taken. NCOEF on the other hand took the value 6 (Tables 2 and 3), 8 (Tables 4 and 5), 9 (Tables 6 and 7) and 12 (Tables 8 and 9). Denoting the function to be modelled by $\alpha(\phi)$:

$$\alpha(\phi) \doteq K(\phi)_1 - K_a(\phi)_1 \tag{42}$$

and the B-spline approximation by $\beta(\phi)$, the error was defined by

$$\text{error} \doteq \frac{\max_i |\alpha_i(\phi) - \beta_i(\phi)|}{\max_i |\alpha_i(\phi)|} (\%), \tag{43}$$

where i represents the data points at which $K(\phi)_1$ was calculated (about 100 points uniformly distributed in the interval $0 < \phi < \pi$. The error made by the B-spline approximation was generally very small (predominantly $< 1\%$). The B-splines can be evaluated using the IMSL subroutine DBSVAL.

Table 4. BSCOEF (NCOEF = 8)

	BSCOEF(1)	BSCOEF(2)	BSCOEF(3)	BSCOEF(4)	BSCOEF(5)	BSCOEF(6)	BSCOEF(7)	BSCOEF(8)
10	−40.5475	0.0190	−0.0696	−0.1447	−0.1447	−0.0700	0.0178	−0.8752
13	−9.3562	0.0212	−0.0766	−0.1574	−0.1435	−0.0665	0.0163	−0.3718
19	−0.0663	0.0219	−0.0782	−0.1743	−0.1859	−0.1342	−0.0614	0.0244
25	−0.3082	0.0200	−0.0821	−0.1485	−0.1189	−0.0565	0.0128	−0.3472
30	0.0139	−0.0200	−0.0523	−0.0710	−0.0706	−0.0516	−0.0198	0.0139
35	−0.3787	0.0170	−0.0531	−0.1139	−0.1120	−0.0763	−0.0296	0.0169
37	−0.1209	0.0263	−0.0921	−0.1649	−0.1581	−0.1065	−0.0450	0.0190
39	−0.1396	0.0369	−0.0195	−0.2196	−0.2461	−0.1521	−0.0688	0.0210
40	0.0087	−0.0059	−0.0226	−0.0432	−0.0505	−0.0322	−0.0057	0.0087
45	−0.0568	0.0088	−0.0180	−0.0894	−0.0948	−0.0621	−0.0243	0.0135
49	−0.2215	0.0505	−0.0198	−0.2654	−0.2954	−0.1804	−0.0822	0.0207
51	0.0049	−0.0012	−0.0040	−0.0158	−0.0363	−0.0261	−0.0033	0.0069
52	0.0030	−0.0011	−0.0003	−0.0103	−0.0396	−0.0336	−0.0088	0.0068
54	−0.0072	0.0124	−0.0119	−0.0498	−0.0532	−0.0351	−0.0123	0.0094
55	−0.0110	0.0138	−0.0086	−0.0669	−0.0729	−0.0464	−0.0157	0.0110
56	−0.0308	0.0078	0.0004	−0.0966	−0.1047	−0.0660	−0.0261	0.0124
57	−0.0948	0.0158	−0.0114	−0.1476	−0.1569	−0.0966	−0.0398	0.0148
58	−0.1757	0.0389	−0.0398	−0.2267	−0.2409	−0.1479	−0.0635	0.0181
59	−0.3009	0.0755	−0.0757	−0.3000	−0.3679	−0.2514	−0.1144	0.0199
60	0.0062	−0.0016	−0.0013	−0.0166	−0.0163	−0.0012	−0.0017	0.0061
65	−0.0324	0.0343	0.0155	−0.0409	−0.0514	−0.0348	−0.0143	0.0079
69	−0.4822	0.1019	−0.0520	−0.4225	−0.4597	−0.2836	−0.1227	0.0238
70	0.0123	−0.0022	0.0038	−0.0072	−0.0069	0.0037	−0.0021	0.0075
72	0.0164	−0.0055	0.0137	0.0076	−0.0136	−0.0083	−0.0023	0.0045
77	−0.1610	0.0923	0.0624	−0.0713	−0.1033	−0.0731	−0.0351	0.0087
78	0.2874	0.0788	0.0606	−0.1946	−0.2419	−0.1605	−0.0706	0.0142
79	−0.7580	0.1259	−0.0200	−0.5292	−0.5936	−0.3776	−0.1592	0.0268
89	−1.2608	0.4872	−0.5188	−0.6738	−0.6541	−0.4223	−0.1777	0.0299
93	0.0476	−0.0086	0.0167	0.0174	−0.0007	−0.0017	−0.0018	0.0018
94	0.0390	−0.0139	0.0242	0.0271	0.0000	−0.0030	−0.0033	0.0015
95	0.3076	−0.0297	0.0384	0.0428	0.0038	−0.0044	−0.0058	0.0012
97	3.6371	−0.1609	0.0980	0.1292	0.0110	−0.0222	−0.0109	0.0008
X1	−0.7006	0.0202	−0.0725	−0.1838	−0.1827	−0.0725	0.0174	−0.0719
E1	−0.3804	0.0984	−0.0594	−0.4428	−0.4655	−0.2770	−0.1281	0.0242
E3	−0.3752	0.0985	−0.0563	−0.4310	−0.4421	−0.2499	−0.1220	0.0218
G1	−1.0457	0.4408	−0.9182	−1.1266	−1.0446	−0.6469	−0.2859	0.0457
G2	−1.4970	0.4030	−0.0886	−1.0243	−1.1406	−0.7105	−0.3163	0.0436
G3	−2.9186	0.3386	0.0064	−0.9880	−1.0964	−0.6652	−0.3056	0.0417
I1	−68.2380	15.5035	−0.2951	−6.1477	−6.8432	−4.3993	−1.9668	0.2288
I3	−129.4787	9.4629	−4.2331	−5.5838	−4.7772	−2.8671	−1.0832	0.1806

Table 5. XKNOT and error values (NCOEF = 8)

	XKNOT(4)	XKNOT(5)	XKNOT(6)	XKNOT(7)	XKNOT(8)	XKNOT(9)	Error (%)
10	−0.100	0.004	0.965	2.178	3.124	3.242	0.309
13	−0.100	0.008	0.960	2.184	3.118	3.242	0.284
19	−0.100	0.066	0.763	1.514	2.150	3.242	1.023
25	−0.100	0.031	0.975	2.156	3.122	3.242	0.306
30	−0.100	0.616	1.267	1.902	2.530	3.242	0.957
35	−0.100	0.027	0.805	1.655	2.426	3.242	0.687
37	−0.100	0.059	0.812	1.448	2.235	3.242	0.489
39	−0.100	0.064	0.205	1.145	1.960	3.242	0.352
40	−0.100	0.370	0.857	1.733	2.777	3.242	0.733
45	−0.100	0.053	0.581	1.621	2.428	3.242	0.473
49	−0.100	0.060	0.184	1.005	1.775	3.242	0.289
51	−0.100	0.182	0.622	1.052	2.860	3.242	0.493
52	−0.100	0.171	0.479	0.786	2.623	3.242	0.568
54	−0.100	0.487	0.813	1.791	2.592	3.242	0.646
55	−0.100	0.354	0.627	1.637	2.546	3.242	1.781
56	−0.100	0.114	0.484	1.484	2.342	3.242	0.385
57	−0.100	0.070	0.412	1.306	2.164	3.242	0.310
58	−0.100	0.067	0.346	1.102	1.916	3.242	0.257
59	−0.100	0.064	0.303	0.747	1.348	3.242	0.456
60	−0.100	0.144	0.933	2.233	2.994	3.242	0.500
65	−0.100	0.385	0.627	1.601	2.453	3.242	1.443
69	−0.100	0.061	0.219	0.797	1.456	3.242	0.765
70	−0.100	0.089	0.937	2.229	3.025	3.242	2.035
72	−0.100	0.077	0.557	1.029	2.884	3.242	0.641
77	−0.100	0.236	0.423	1.089	1.828	3.242	0.863
78	−0.100	0.138	0.305	0.887	1.546	3.242	0.340
79	−0.100	0.064	0.204	0.688	1.251	3.242	0.886
89	−0.100	0.132	0.550	0.745	1.231	3.242	0.952
93	−0.100	0.050	0.458	0.839	2.776	3.242	1.367
94	−0.100	0.060	0.365	0.680	2.489	3.242	0.514
95	−0.100	0.031	0.311	0.577	1.990	3.242	0.803
97	−0.100	0.017	0.168	0.331	1.257	3.242	0.800
X1	−0.100	0.022	0.904	2.255	3.089	3.242	0.131
E1	−0.100	0.063	0.222	0.807	1.409	3.242	0.236
E3	−0.100	0.063	0.212	0.776	1.326	3.242	0.241
G1	−0.100	0.077	0.448	0.677	1.106	3.242	0.317
G2	−0.100	0.060	0.130	0.465	0.863	3.242	0.215
G3	−0.100	0.039	0.111	0.450	0.820	3.242	0.201
I1	−0.100	0.046	0.048	0.194	0.418	3.242	0.300
I3	−0.100	0.023	0.133	0.257	1.164	3.242	0.273

Table 6. BSCOEF (NCOEF = 9)

	BSCOEF(1)	BSCOEF(2)	BSCOEF(3)	BSCOEF(4)	BSCOEF(5)	BSCOEF(6)	BSCOEF(7)	BSCOEF(8)	BSCOEF(9)
15	−0.0652	0.0190	−0.0503	−0.1060	−0.1467	−0.1613	−0.1310	−0.0611	0.0248
20	−0.5490	0.0141	−0.0369	−0.0894	−0.1082	−0.0869	−0.0349	0.0134	−0.1865
32	−0.1271	0.0100	−0.0208	−0.0706	−0.0825	−0.0584	−0.0223	0.0095	−0.2004
33	−0.1584	0.0113	−0.0221	−0.0790	−0.0901	−0.0633	−0.0250	0.0099	−0.3187
50	0.0059	−0.0020	−0.0087	−0.0207	−0.0305	−0.0266	−0.0096	−0.0019	0.0060
53	−0.0005	−0.0004	0.0028	−0.0110	−0.0406	−0.0421	−0.0249	−0.0076	0.0086
73	0.0243	−0.0091	0.0204	0.0150	−0.0099	−0.0145	−0.0090	−0.0032	0.0050
74	0.7078	−0.0194	0.0311	0.0236	−0.0116	−0.0205	−0.0146	−0.0052	0.0053
75	0.0788	−0.0261	0.0403	0.0364	−0.0191	−0.0312	−0.0216	−0.0072	0.0060
76	0.2329	−0.0461	0.0596	0.0474	−0.0318	−0.0530	−0.0367	−0.0168	0.0068
80	0.0056	−0.0023	0.0048	0.0018	−0.0018	0.0013	0.0050	−0.0023	0.0059
85	0.4915	−0.0351	0.0492	0.0456	0.0017	−0.0144	−0.0124	−0.0056	0.0039
90	0.0045	−0.0019	0.0044	0.0034	0.0011	0.0032	0.0046	−0.0019	0.0049
91	0.0078	−0.0029	0.0076	0.0064	0.0016	0.0011	0.0021	−0.0014	0.0033
92	0.0136	−0.0048	0.0096	0.0115	0.0072	−0.0009	0.0005	−0.0013	0.0030
96	0.4611	−0.0588	0.0650	0.0696	0.0162	−0.0052	−0.0073	−0.0050	0.0022
98	0.6474	−0.4035	0.2297	0.2467	0.0253	−0.0503	−0.0484	−0.0228	0.0035
99	−1.3121	−1.5915	0.6092	0.4766	−0.2936	−0.5042	−0.3468	−0.1393	0.0187

Table 7. XKNOT and error values (NCOEF = 9)

	XKNOT(4)	XKNOT(5)	XKNOT(6)	XKNOT(7)	XKNOT(8)	XKNOT(9)	XKNOT(10)	Error(%)
15	−0.100	0.061	0.589	0.871	1.411	2.174	3.242	1.172
20	−0.100	0.019	0.666	1.610	2.514	3.112	3.242	0.153
32	−0.100	0.031	0.525	1.716	2.580	3.120	3.242	0.221
33	−0.100	0.031	0.513	1.675	2.538	3.124	3.242	0.186
50	−0.100	0.234	0.766	1.275	2.269	2.917	3.242	0.408
53	−0.100	0.184	0.426	0.807	0.038	2.724	3.242	1.090
73	−0.100	0.067	0.461	0.843	2.102	2.830	3.242	0.594
74	−0.100	0.019	0.406	0.737	1.831	2.712	3.242	0.592
75	−0.100	0.045	0.310	0.576	1.683	2.639	3.242	1.054
76	−0.100	0.030	0.270	0.501	1.357	2.271	3.242	0.461
80	−0.100	0.128	0.769	1.503	2.338	3.018	3.242	2.094
85	−0.100	0.026	0.331	0.624	1.578	2.589	3.242	0.445
90	−0.100	0.125	0.764	1.512	2.350	3.024	3.242	2.573
91	−0.100	0.095	0.663	1.247	2.220	2.984	3.242	0.859
92	−0.100	0.080	0.471	0.761	1.331	2.957	3.242	0.435
96	−0.100	0.030	0.255	0.487	1.368	2.393	3.242	0.740
98	−0.100	0.030	0.123	0.249	0.743	1.360	3.242	0.308
99	−0.100	0.052	0.052	0.134	0.455	0.927	3.242	0.636

Table 8. BSCOEF (NCOEF = 12)

	BSCOEF(1)	BSCOEF(2)	BSCOEF(3)	BSCOEF(4)	BSCOEF(5)	BSCOEF(6)	BSCOEF(7)	BSCOEF(8)	BSCOEF(9)	BSCOEF(10)	BSCOEF(11)	BSCOEF(12)
71	0.0682	−0.0107	0.0007	0.0005	0.0077	0.0013	−0.0078	−0.0070	−0.0020	−0.0018	−0.0006	0.0062

Table 9. XKNOT and error values (NCOEF = 12)

	XKNOT(4)	XKNOT(5)	XKNOT(6)	XKNOT(7)	XKNOT(8)	XKNOT(9)	XKNOT(10)	XKNOT(11)	XKNOT(12)	XKNOT(13)	Error (%)
71	−0.100	0.049	0.067	0.075	0.703	1.290	2.243	2.901	3.032	3.242	1.384

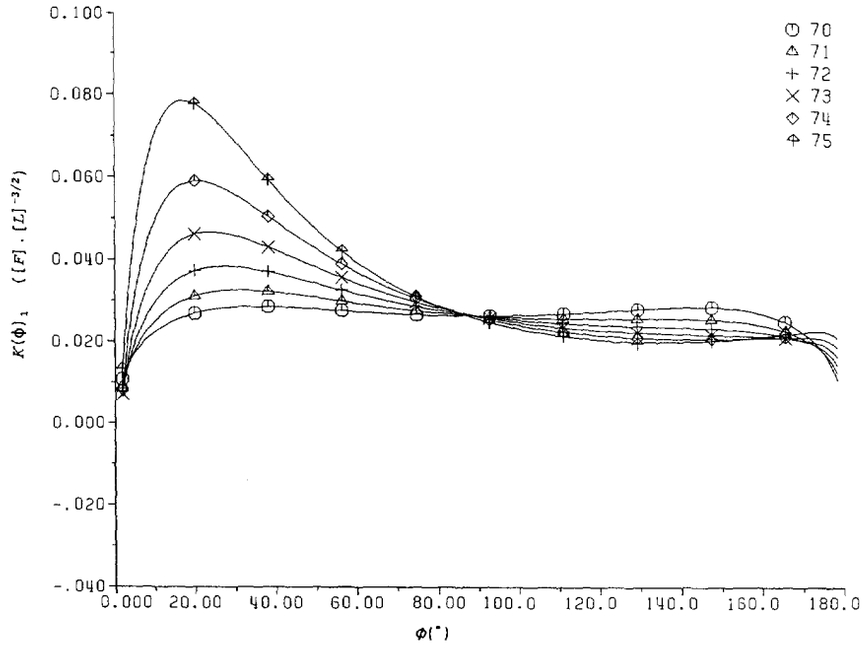

Fig. 26. $K(\phi)_I$ along $\rho_0 = 0.7$ [L] (point force positions 70 → 75).

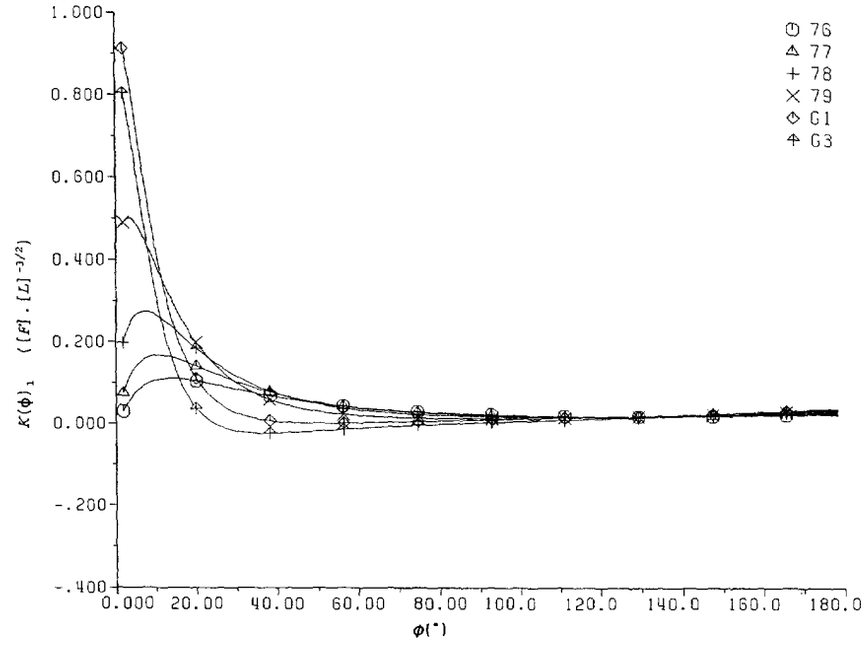

Fig. 27. $K(\phi)_I$ along $\rho_0 = 0.7$ [L] (point force positions 76 → G3).

Figures 26 and 27 show the $K(\phi)_I$ distribution for point loads on a circle with radius 0.7 [L]. Each of the curves exhibits the behaviour discussed in Section 3: $K(\phi)_I$ grows towards the free surface ($\phi = 0, \pi$), reaching a maximum before falling off rapidly at the free surface. As the point force approaches the free surface at $\phi = 0$ (position 70 → G3), so does the $K(\phi)_I$ maximum nearest to $\phi = 0$, while growing continuously, except perhaps for point forces immediately at the free surface (transition G1 → G3).

Figure 28 illustrates the $K(\phi)_I$ behaviour along the line $\phi_0 = \pi/4$. Each curve separately agrees with previous findings. For a point force approaching the crack front (position 15 → 95), Fig. 28 illustrates that $K(\phi)_I$ near the free boundary continuously decreases, while

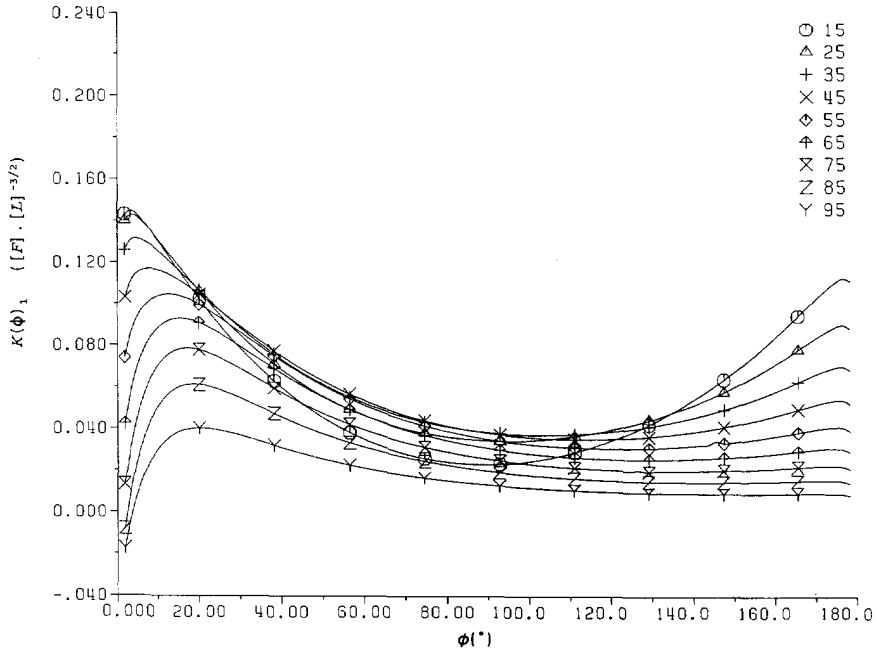

Fig. 28. $K(\phi)_1$ along $\phi = \pi/4$.

$K(\pi/2)_1$ at first increases and then decreases again, illustrating the influence of the distance between the load application point and the boundary point at which $K(\phi)_1$ is calculated.

6. CONCLUSIONS

The Green function was calculated for a series of representative point load positions on the faces of a half circular crack in half infinite space. It was shown that the stress intensity factor increases towards the free surface, but drops quite sharply at the free surface. A general theoretical investigation of the zero and first iterations leads to a zero K-value at an infinitesimal distance away from the free surface.

REFERENCES

Becker, I. (1989). Numerische Berechnung von Ecken- und Kantensingularitäten elastischer Felder für dreidimensionale Rißprobleme. Dissertation, Universität Karlsruhe.

Bender, C. M. and Orszag, S. A. (1978). *Advanced Mathematical Methods for Scientists and Engineers*. McGraw-Hill, New York.

Benthem, J. P. (1977). State of stress at the vertex of a quarter-infinite crack in a half-space. *Int. J. Solids Structures* **13,** 479–492.

Benthem, J. P. (1980). The quarter-infinite crack in a half space; alternative and additional solutions. *Int. J. Solids Structures* **16,** 119–130.

Fabrikant, V. I. (1988). Green's functions for a penny-shaped crack under normal loading. *Engng Fracture Mech.* **30,** 87–104.

Gao, H. and Rice, J. R. (1987). Somewhat circular tensile cracks. *Int. J. Fracture* **33,** 155–174.

Gradshteyn, I. S. and Ryzhik, I. M. (1980). *Table of Integrals, Series and Products*, Corrected and enlarged edition. Academic Press, New York.

Hahn, H. G. (1976). *Bruchmechanik*. Teubner Studienbücher Mechanik.

Hartranft, R. J. and Sih, G. C. (1973). Alternating method applied to edge and surface crack problems. In *Methods of Analysis and Solutions of Crack Problems* (Edited by G. C. Sih), pp. 179–238. Noordhoff Internat., Leyden.

IMSL Math/Library. (1989). *FORTRAN Subroutines for Mathematical Applications*, Version 1.1.

Kantarovich, L. V. and Krylov, V. I. (1964). *Approximate Methods of Higher Analysis*. Interscience, New York.

Muki, R. (1960). *Progress in Solid Mechanics*, Vol. 1, p. 401. North-Holland, Amsterdam.

Piessens, R., de Doncker-Kapenga, E., Überhuber, C. W. and Kahaner, D. K. (1983). *Quadpack. A Subroutine Package for Automatic Integration*. Springer, Berlin.

Sloan, S. W. and Houlsby, G. T. (1983). An implementation of Watson's algorithm for computing 2-dimensional Delaunay triangulations. University of Oxford, Soil Mechanics Report No. SM045/83.

Smith, C. W. (1988). Measurement of three-dimensional effects in fracture mechanics. In *Fracture Mechanics: Nineteenth Symposium* (Edited by T. A. Cruse), ASTM STP 969, pp. 5–18. Society for Testing of Materials, Philadelphia.

Smith, F. W., Emery, A. F. and Kobayashi, A. S. (1967a). Stress intensity factors for semicircular cracks. *J. Appl. Mech.* **34,** 953–959.
Smith, F. W., Kobayashi, A. S. and Emery, A. F. (1967b). Stress intensity factors for penny-shaped cracks. *J. Appl. Mech.* **34,** 947–952.
Tada, H. (1973). *The Stress Analysis of Cracks Handbook*. Del Research Corporation.
Timoshenko, S. P. and Goodier, J. N. (1970). *Theory of Elasticity*, 3rd edn. McGraw-Hill, New York.

APPENDIX A: GREEN FUNCTIONS FOR A PENNY-SHAPED CRACK UNDER NORMAL LOADING FOR A LINEAR ELASTIC ISOTROPIC MATERIAL

Consider a penny-shaped crack opened by two equal concentrated forces P applied in opposite directions at the point Q_0 $(\rho_0, \phi_0, 0^{\pm})$, $\rho_0 < a$ (Fig. A1). The Green functions for a transversely isotropic body in a point $Q(\rho, \phi, z)$, $z \geqslant 0$ are (Fabrikant, 1988) (the solutions for $z < 0$ follow from symmetry considerations):

$$u = \frac{2}{\pi} HP\left[\frac{\gamma_1}{m_1 - 1} f_1(z_1) + \frac{\gamma_2}{m_2 - 1} f_1(z_2)\right] \tag{A1}$$

$$u_z = w = \frac{2}{\pi} HP\left[\frac{m_1}{m_1 - 1} f_2(z_1) + \frac{m_2}{m_2 - 1} f_2(z_2)\right] \tag{A2}$$

$$\sigma_1 = \frac{2P}{\pi^2(\gamma_1 - \gamma_2)}\left\{\left[\frac{\gamma_1}{(m_1 + 1)\gamma_3^2} - \frac{1}{\gamma_1}\right] f_3(z_1) - \left[\frac{\gamma_2}{(m_2 + 1)\gamma_3^2} - \frac{1}{\gamma_2}\right] f_3(z_2)\right\} \tag{A3}$$

$$\sigma_2 = \frac{4}{\pi} HA_{66}P\left[\frac{\gamma_1}{m_1 - 1} f_4(z_1) + \frac{\gamma_2}{m_2 - 1} f_4(z_2)\right] \tag{A4}$$

$$\sigma_z = \frac{P}{\pi^2(\gamma_1 - \gamma_2)}[\gamma_1 f_3(z_1) - \gamma_2 f_3(z_2)] \tag{A5}$$

$$\tau_z = \frac{P}{\pi^2(\gamma_1 - \gamma_2)}[f_5(z_1) - f_5(z_2)], \tag{A6}$$

where

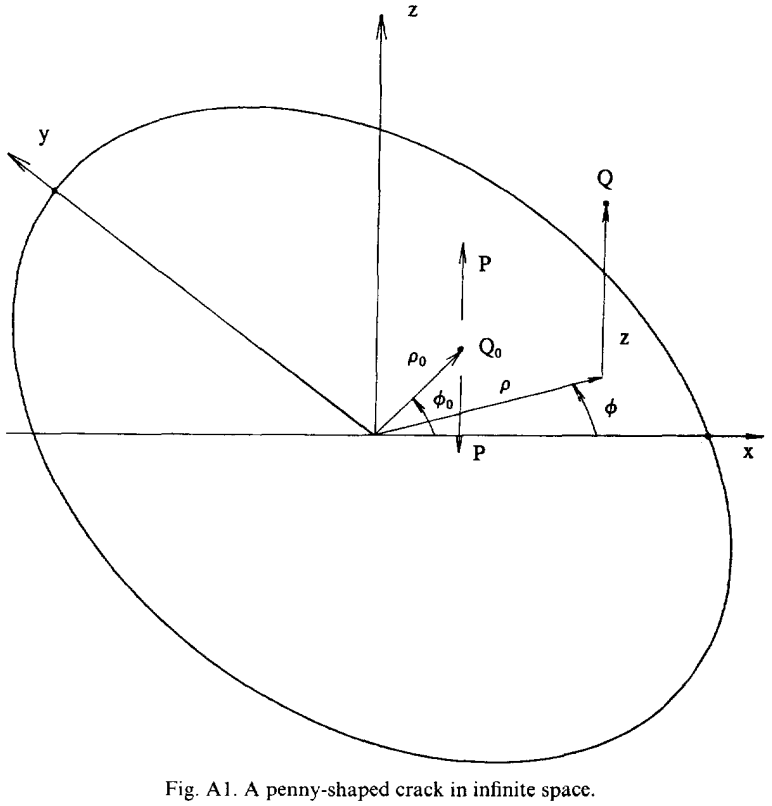

Fig. A1. A penny-shaped crack in infinite space.

$$f_1(z) = \frac{1}{\bar{q}}\left[\frac{(a^2-\rho_0^2)^{1/2}}{\bar{s}}\tan^{-1}\left(\frac{\bar{s}}{(l_2^2-a^2)^{1/2}}\right) - \frac{z}{R_0}\tan^{-1}\left(\frac{h}{R_0}\right)\right] \tag{A7}$$

$$f_2(z) = \frac{1}{R_0}\tan^{-1}\left(\frac{h}{R_0}\right) \tag{A8}$$

$$f_3(z) = \left\{-\frac{z}{R_0^3}\tan^{-1}\left(\frac{h}{R_0}\right) + \frac{h}{z(R_0^2+h^2)}\left[\frac{\rho^2-l_1^2}{l_2^2-l_1^2} - \frac{z^2}{R_0^2}\right]\right\} \tag{A9}$$

$$f_4(z) = \frac{(a^2-\rho_0^2)^{1/2}}{\bar{q}\,\bar{s}}\left(\frac{\rho_0 e^{i\phi_0}}{\bar{s}^2} - \frac{2}{\bar{q}}\right)\tan^{-1}\left(\frac{\bar{s}}{(l_2^2-a^2)^{1/2}}\right) + \frac{z(3R_0^2-z^2)}{\bar{q}^2 R_0^3}\tan^{-1}\left(\frac{h}{R_0}\right)$$
$$- \frac{(a^2-\rho_0^2)^{1/2}(l_2^2-a^2)^{1/2}\rho_0 e^{i\phi_0}}{\bar{q}\,\bar{s}^2[l_2^2-\rho\rho_0 e^{-i(\phi-\phi_0)}]} + \frac{zh}{R_0^2+h^2}\left[\frac{q}{\bar{q}R_0^2} - \frac{\rho^2 e^{2i\phi}}{(l_2^2-l_1^2)(l_2^2-\rho^2)}\right] \tag{A10}$$

$$f_5(z) = -\left\{\frac{\rho e^{i\phi}-\rho_0 e^{i\phi_0}}{R_0^3}\tan^{-1}\left(\frac{h}{R_0}\right) + \frac{h}{R_0^2+h^2}\left[\frac{\rho e^{i\phi}}{l_2^2-l_1^2} + \frac{\rho e^{i\phi}-\rho_0 e^{i\phi_0}}{R_0^2}\right]\right\} \tag{A11}$$

and

$$z_k = z/\gamma_k \quad (k = 1, 2, 3) \tag{A12}$$

$$l_1 = \tfrac{1}{2}\{\sqrt{(\rho+a)^2+z^2} - \sqrt{(\rho-a)^2+z^2}\} \tag{A13}$$

$$l_2 = \tfrac{1}{2}\{\sqrt{(\rho+a)^2+z^2} + \sqrt{(\rho-a)^2+z^2}\} \tag{A14}$$

$$R_0 = \sqrt{\rho^2+\rho_0^2-2\rho\rho_0\cos(\phi-\phi_0)+z^2} \tag{A15}$$

$$h = \frac{1}{a}\sqrt{a^2-l_1^2}\sqrt{a^2-\rho_0^2}. \tag{A16}$$

The material parameters γ_1, γ_2, γ_3, m_1, m_2 and H are defined by

$$\bar{q} = \rho e^{-i\phi} - \rho_0 e^{-i\phi_0}, \quad \bar{s} = \sqrt{a^2-\rho\rho_0 e^{-i(\phi-\phi_0)}} \tag{A17}$$

$$\frac{A_{44}+m_k(A_{13}+A_{44})}{A_{11}} = \frac{m_k A_{33}}{m_k A_{44}+A_{13}+A_{44}} = \gamma_k^2 \quad (k = 1, 2 \wedge \gamma_1, \gamma_2 \geqslant 0), \quad \gamma_3 = \sqrt{A_{44}/A_{66}} \tag{A18}$$

$$H = \frac{(\gamma_1+\gamma_2)A_{11}}{2\pi(A_{11}A_{33}-A_{13}^2)}, \tag{A19}$$

where A_{11}, A_{13}, A_{33}, A_{44} and A_{66} are the five elastic constants characterizing the transversely isotropic linear elastic material by the following stress–strain relationships:

$$\sigma_x = A_{11}\frac{\partial u_x}{\partial x} + (A_{11}-2A_{66})\frac{\partial u_y}{\partial y} + A_{13}\frac{\partial w}{\partial z} \tag{A20}$$

$$\sigma_y = (A_{11}-2A_{66})\frac{\partial u_x}{\partial x} + A_{11}\frac{\partial u_y}{\partial y} + A_{13}\frac{\partial w}{\partial z} \tag{A21}$$

$$\sigma_z = A_{13}\frac{\partial u_x}{\partial x} + A_{13}\frac{\partial u_y}{\partial y} + A_{33}\frac{\partial w}{\partial z} \tag{A22}$$

$$\tau_{xy} = A_{66}\left(\frac{\partial u_x}{\partial y} + \frac{\partial u_y}{\partial x}\right), \quad \tau_{yz} = A_{44}\left(\frac{\partial u_y}{\partial z} + \frac{\partial w}{\partial y}\right), \quad \tau_{zx} = A_{44}\left(\frac{\partial w}{\partial x} + \frac{\partial u_x}{\partial z}\right). \tag{A23}$$

The stresses and displacements in Cartesian coordinates can be obtained from:

$$\sigma_1 = \sigma_x + \sigma_y \tag{A24}$$

$$\sigma_2 = \sigma_x - \sigma_y + 2i\tau_{xy} \tag{A25}$$

$$\tau_z = \tau_{zx} + i\tau_{yz} \tag{A26}$$

$$u = u_x + iu_y. \tag{A27}$$

For a linear elastic isotropic material the material constants reduce to:

$$A_{11} = A_{33} = \lambda + 2\mu \tag{A28}$$

$$A_{44} = A_{66} = \mu \tag{A29}$$

$$A_{13} = \lambda, \tag{A30}$$

where λ is Lamé's constant and μ is the shear modulus. Application of eqn (A18) yields:

$$m_1 = m_2 = 1 \tag{A31}$$

and

$$\gamma_1 = \gamma_2 = \gamma_3 = 1 \tag{A32}$$

$$H = \frac{\lambda + 2\mu}{4\mu\pi(\lambda + \mu)} = \frac{1 - \nu}{2\mu\pi}; \tag{A33}$$

ν is Poisson's coefficient. Substituting these constants into eqns (A1)–(A6) leads to indeterminate expressions. This problem can be solved by considering a slightly anisotropic material and taking the limit. Indeed, the general solution of the first equality in eqn (A18) yields:

$$m_k = -b \pm \sqrt{b^2 - 1}, \tag{A34}$$

where

$$b = \frac{(A_{13} + A_{44})^2 + A_{44}^2 - A_{33}A_{11}}{2A_{44}(A_{13} + A_{44})}; \tag{A35}$$

$b = -1$ for an isotropic material. Let

$$A_{11} = \lambda + 2\mu + \varepsilon D_{11} \tag{A36}$$

$$A_{13} = \lambda + \varepsilon D_{13} \tag{A37}$$

$$A_{33} = \lambda + 2\mu + \varepsilon D_{33} \tag{A38}$$

$$A_{44} = \mu + \varepsilon D_{44} \tag{A39}$$

$$A_{66} = \mu + \varepsilon D_{66}, \tag{A40}$$

where $\varepsilon \ll 1$. Then

$$b \sim -1 - \varepsilon N, \quad \varepsilon \to 0, \tag{A41}$$

where

$$N = -\frac{1}{2\lambda(\lambda + \mu)} \left\{ [2(\lambda + \mu)(D_{13} + D_{44}) + 2\mu D_{44} - (\lambda + 2\mu)(D_{11} + D_{33})] + \frac{2\mu}{\lambda} [\mu(D_{13} + D_{44}) + (\lambda + \mu)D_{44}] \right\}. \tag{A42}$$

Substitution of eqn (A41) into eqn (A34) yields:

$$m_{1,2} \sim 1 \pm \sqrt{2\varepsilon N} + \varepsilon N + O(\varepsilon\sqrt{\varepsilon}), \quad \varepsilon \to 0. \tag{A43}$$

Using eqn (A43), γ_1 and γ_2 take the values:

$$\gamma_1 \sim 1 + \Gamma\sqrt{2\varepsilon N}, \quad \varepsilon \to 0 \tag{A44}$$

$$\gamma_2 \sim 1 - \Gamma\sqrt{2\varepsilon N}, \quad \varepsilon \to 0, \tag{A45}$$

where

$$\Gamma = \frac{(\lambda+\mu)}{2(\lambda+2\mu)} = \frac{1}{4(1-\nu)}. \tag{A46}$$

Analogously, γ_3 can be written as:

$$\gamma_3 \sim 1 + \frac{\varepsilon M}{2}, \quad \varepsilon \to 0, \tag{A47}$$

where

$$M = \frac{1}{\mu}(D_{44} - D_{66}). \tag{A48}$$

By means of eqns (A43)–(A48), σ_1 in eqn (A3) can be shown to satisfy:

$$\sigma_1 \sim \frac{2P}{\pi^2}\left\{\frac{z f'_3(z)}{2} + \frac{1}{4}\left(\frac{6\Gamma-1}{\Gamma}\right) f_3(z)\right\}, \quad \varepsilon \to 0, \tag{A49}$$

where

$$\frac{6\Gamma-1}{\Gamma} = 2(1+2\nu). \tag{A50}$$

In the same way one arrives at:

$$\sigma_2 \sim -\frac{P}{\pi^2}\{(1-2\nu) f_4(z) + z f'_4(z)\}, \quad \varepsilon \to 0 \tag{A51}$$

$$\sigma_z \sim \frac{P}{\pi^2}\{f_3(z) - z f'_3(z)\}, \quad \varepsilon \to 0 \tag{A52}$$

$$\tau_z \sim -\frac{P}{\pi^2} z f'_5(z), \quad \varepsilon \to 0 \tag{A53}$$

$$u \sim \frac{4\Gamma}{\pi} H P\{(2\nu-1) f_1(z) - z f'_1(z)\}, \quad \varepsilon \to 0 \tag{A54}$$

$$w \sim \frac{4}{\pi} H P\{\tfrac{1}{2} f_2(z) - z\Gamma f'_2(z)\}, \quad \varepsilon \to 0. \tag{A55}$$

Equations (A49)–(A55) reveal the need for analytical expressions for $f'_1(z)$ up to $f'_5(z)$. The calculation is rather long and tedious. They take the form:

$$f'_1(z) = \frac{1}{\bar{q}}\left\{\frac{\sqrt{a^2-\rho_0^2}}{\bar{s}} \frac{-1}{[l_2^2 - a^2 + \bar{s}^2]} \frac{z\bar{s} l_2^2}{L\sqrt{l_2^2 - a^2}}\right\}$$
$$- \frac{1}{\bar{q}}\left\{\frac{R_0 - z^2/R_0}{R_0^2}\tan^{-1}\left(\frac{h}{R_0}\right) - \frac{z^2 h}{R_0(R_0^2+h^2)}\left[\frac{l_1^2 R_0}{L(a^2-l_1^2)} - \frac{1}{R_0}\right]\right\} \tag{A56}$$

$$f'_2(z) = -\frac{z}{R_0^3}\tan^{-1}\left(\frac{h}{R_0}\right) + \frac{z h}{R_0(R_0^2+h^2)}\left[\frac{l_1^2 R_0}{L(a^2-l_1^2)} - \frac{1}{R_0}\right] \tag{A57}$$

$$f'_3(z) = -\frac{(R_0^2-3z^2)}{R_0^5}\tan^{-1}\left(\frac{h}{R_0}\right) \quad \frac{z^2h}{R_0^3(R_0^2+h^2)}\left[\frac{l_1^2R_0}{L(a^2-l_1^2)}-\frac{1}{R_0}\right]+\frac{1}{z^2(R_0^2+h^2)^2}$$
$$\cdot\left[\frac{\rho^2-l_1^2}{l_2^2-l_1^2}-\frac{z^2}{R_0^2}\right]\left\{\frac{z^2l_1^2h(R_0^2+h^2)}{L(a^2-l_1^2)}-h\left[R_0^2+h^2+2z^2\left(1+\frac{h^2l_1^2}{L(a^2-l_1^2)}\right)\right]\right\}$$
$$+\frac{2h}{(R_0^2+h^2)}\left[\frac{-1}{L(l_2^2-l_1^2)^2}[\rho^2(l_1^2+l_2^2)-2l_1^2l_2^2]-\left(\frac{R_0^2-z^2}{R_0^4}\right)\right] \tag{A58}$$

$$f'_4(z) = -\frac{\sqrt{a^2-\rho_0^2}}{\bar{q}}\left(\frac{\rho_0\,e^{i\phi_0}}{\bar{s}^2}-\frac{2}{\bar{q}}\right)\frac{1}{[l_2^2-a^2+\bar{s}^2]}\frac{l_2^2z}{L\sqrt{l_2^2-a^2}}$$
$$+\frac{z^2(3R_0^2-z^2)h}{\bar{q}^2R_0^3}\frac{1}{(R_0^2+h^2)}\left[\frac{l_1^2R_0}{L(a^2-l_1^2)}-\frac{1}{R_0}\right]+\frac{3(R_0^2-z^2)^2}{\bar{q}^2R_0^5}\tan^{-1}\left(\frac{h}{R_0}\right)$$
$$+\frac{\rho_0\,e^{i\phi_0}\sqrt{a^2-\rho_0^2}}{\bar{q}\bar{s}^2}\frac{zl_2^2[l_2^2-2a^2+\rho\rho_0\,e^{-i(\phi-\phi_0)}]}{L\sqrt{l_2^2-a^2}\,[l_2^2-\rho\rho_0\,e^{-i(\phi-\phi_0)}]^2}$$
$$+\frac{zh}{(R_0^2+h^2)}\left\{-\frac{2zq}{\bar{q}R_0^4}+\frac{\rho^2\,e^{2i\phi}[2z(2l_2^4-\rho^2(l_2^2+l_1^2))]}{L(l_2^2-l_1^2)^2(l_2^2-\rho^2)^2}\right\}$$
$$+\left\{\frac{h[(R_0^2+h^2)-2z^2]}{(R_0^2+h^2)^2}+\frac{z^2l_1^2h[R_0^2-h^2]}{(R_0^2+h^2)^2(a^2-l_1^2)L}\right\}\left[\frac{q}{\bar{q}R_0^2}-\frac{\rho^2\,e^{2i\phi}}{(l_2^2-l_1^2)(l_2^2-\rho^2)}\right] \tag{A59}$$

$$f'_5(z) = \frac{3z}{R_0^5}(\rho\,e^{i\phi}-\rho_0\,e^{i\phi_0})\tan^{-1}\left(\frac{h}{R_0}\right)-\left[\frac{\rho\,e^{i\phi}-\rho_0\,e^{i\phi_0}}{R_0^3}\right]\frac{zh}{(R_0^2+h^2)}\left[\frac{l_1^2R_0}{L(a^2-l_1^2)}-\frac{1}{R_0}\right]$$
$$-\frac{1}{(R_0^2+h^2)^2}\left[\frac{zl_1^2h(R_0^2+h^2)}{L(a^2-l_1^2)}-h\left(2z+\frac{2h^2zl_1^2}{L(a^2-l_1^2)}\right)\right]\left\{\frac{\rho\,e^{i\phi}}{l_2^2-l_1^2}+\frac{\rho\,e^{i\phi}-\rho_0\,e^{i\phi_0}}{R_0^2}\right\}$$
$$+\frac{h}{(R_0^2+h^2)}\left\{\frac{\rho\,e^{i\phi}}{(l_2^2-l_1^2)^2}\frac{2z}{L}(l_1^2+l_2^2)+\frac{2z(\rho\,e^{i\phi}-\rho_0\,e^{i\phi_0})}{R_0^4}\right\}, \tag{A60}$$

where

$$L=\sqrt{(\rho+a)^2+z^2}\cdot\sqrt{(\rho-a)^2+z^2}\,. \tag{A61}$$

APPENDIX B: GREEN FUNCTIONS FOR A PENNY-SHAPED CRACK UNDER NORMAL LOADING IN THE VICINITY OF THE CRACK FRONT

Normal stress $(\sigma_y)_1$

The geometry of the problem is shown in Fig. B1, and can be described by:

$$\phi = 0 \tag{B1}$$

$$\rho = a+\varepsilon\cos\theta,\quad 0\leqslant\theta\leqslant\pi,\quad \varepsilon\ll a \tag{B2}$$

$$z=\varepsilon\sin\theta,\quad \varepsilon\ll a \tag{B3}$$

$$0\leqslant\phi_0\leqslant 2\pi,\quad 0\leqslant\rho_0\leqslant a. \tag{B4}$$

The point Q_0 where the force is applied can be described by (ρ_0, ϕ_0) or equivalently by (R, ψ). They are related by:

$$\rho_0 e^{i\phi_0} = a - Re^{-i\psi}. \tag{B5}$$

Q_0 can be anywhere inside the crack, so

$$-\pi/2\leqslant\psi\leqslant\pi/2,\quad 0\leqslant R\leqslant 2a\cos\psi. \tag{B6}$$

Substitution of the above expressions into eqns (A13)–(A15) yields:

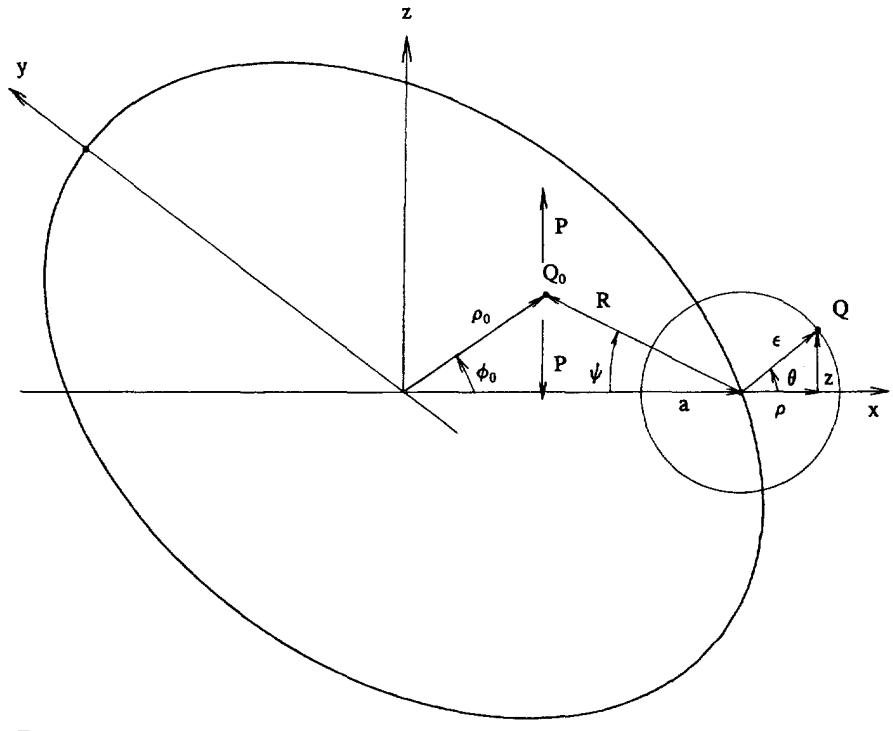

Fig. B1. Geometric parameters used for the determination of the asymptotic expansion of $(\sigma_1)_1$.

$$l_1 = a + \frac{\varepsilon}{2}(\cos\theta - 1) + O(\varepsilon^2), \quad \varepsilon \to 0 \tag{B7}$$

$$l_2 = a + \frac{\varepsilon}{2}(\cos\theta + 1) + O(\varepsilon^2), \quad \varepsilon \to 0 \tag{B8}$$

$$R_0^2 = R^2\left(1 - \frac{R_1}{R}\right)\left(1 - \frac{R_2}{R}\right), \tag{B9}$$

where

$$R_{1,2} = \varepsilon\{-\cos\theta\cos\psi \pm i\sqrt{1 - \cos^2\theta\cos^2\psi}\} \tag{B10}$$

and hence

$$|R_1| = |R_2| = \varepsilon. \tag{B11}$$

Consequently, by Taylor expansion, taking the leading term only, one arrives at:

$$R_0^2 = R^2 + \ldots, \quad R > \varepsilon \tag{B12}$$

$$R_0^2 = \varepsilon^2 + \ldots, \quad R < \varepsilon. \tag{B13}$$

h satisfies:

$$h \sim \sqrt{\frac{(1 - \cos\theta)(2a\cos\psi - R)}{a}}\sqrt{\varepsilon R}, \quad \varepsilon \to 0 \doteq A\sqrt{\varepsilon R}. \tag{B14}$$

Furthermore,

$$R_0^2+h^2 = R^2\left(1-\frac{R_1^*}{R}\right)\left(1-\frac{R_2^*}{R}\right)+\ldots, \quad \varepsilon\to 0, \tag{B15}$$

where

$$R_{1,2}^* = -\varepsilon e^{\pm i\psi} \tag{B16}$$

and hence

$$|R_1^*| = |R_2^*| = \varepsilon. \tag{B17}$$

The Taylor expansion of (B15) yields:

$$R_0^2+h^2 = R^2+\ldots, \quad R>\varepsilon, \quad \varepsilon\to 0 \tag{B18}$$

$$R_0^2+h^2 = \varepsilon^2+\ldots, \quad R<\varepsilon, \quad \varepsilon\to 0. \tag{B19}$$

Another useful relationship is (Gradshteyn and Ryzhik, 1980):

$$\tan^{-1}\left(\frac{h}{R_0}\right) = \frac{h/R_0}{\sqrt{1+(h/R_0)^2}}+\ldots = \frac{h}{\sqrt{h^2+R_0^2}}+\ldots \tag{B20}$$

Substituting eqns (B14), (B18) and (B19) leads to:

$$\tan^{-1}\left(\frac{h}{R_0}\right) = A\frac{\sqrt{\varepsilon}}{\sqrt{R}}+\ldots, \quad R>\varepsilon, \varepsilon\to 0 \tag{B21}$$

$$\tan^{-1}\left(\frac{h}{R_0}\right) = A\frac{\sqrt{R}}{\sqrt{\varepsilon}}+\ldots, \quad R<\varepsilon, \varepsilon\to 0. \tag{B22}$$

$\bar{q}$ takes the form

$$\bar{q} = Re^{i\psi}+\varepsilon\cos\theta = Re^{i\psi}\left(1+\frac{\varepsilon\cos\theta}{Re^{i\psi}}\right), \tag{B23}$$

which by expansion leads to

$$\bar{q} = Re^{i\psi}+\ldots, \quad R>\varepsilon|\cos\theta| \tag{B24}$$

$$\bar{q} = \varepsilon\cos\theta+\ldots, \quad R<\varepsilon|\cos\theta|. \tag{B25}$$

$\bar{s}^2$ satisfies

$$\bar{s}^2 = (a+\varepsilon\cos\theta)Re^{-i\psi}-a\varepsilon\cos\theta \sim aRe^{-i\psi}\left[1-\frac{\varepsilon\cos\theta}{Re^{-i\psi}}\right], \quad \varepsilon\to 0. \tag{B26}$$

Hence, taking the leading term only, one arrives at:

$$\bar{s}^2 = aRe^{-i\psi}+\ldots, \quad R>\varepsilon|\cos\theta|, \quad \varepsilon\to 0 \tag{B27}$$

$$\bar{s}^2 = -a\varepsilon\cos\theta+\ldots, \quad R<\varepsilon|\cos\theta|, \varepsilon\to 0. \tag{B28}$$

Furthermore,

$$\bar{s}^2+l_2^2-a^2 = aRe^{-i\psi}\left[1+\frac{\varepsilon}{Re^{-i\psi}}+O(\varepsilon^2)\right], \quad \varepsilon\to 0 \tag{B29}$$

and consequently

Table B1. Asymptotic expansions as a function of R for $\varepsilon \to 0$

0	Interval I	$\varepsilon\lvert\cos\theta\rvert$	Interval II	ε	Interval III	$2a\cos\psi$
	$h \sim A\sqrt{\varepsilon R}$, $l_1 = a+\varepsilon(\cos\theta-1)/2+\ldots$, $l_2 = a+\varepsilon(\cos\theta+1)/2+\ldots$					
	$R_0^2 = \varepsilon^2+\ldots$ $R_0^2+h^2 = \varepsilon^2+\ldots$ $\tan^{-1}(h/R_0) = A\sqrt{R}/\sqrt{\varepsilon}+\ldots$				$R_0^2 = R^2+\ldots$ $R_0^2+h^2 = R^2+\ldots$ $\tan^{-1}(h/R_0) = A\sqrt{\varepsilon}/\sqrt{R}+\ldots$	
	$\bar{q} = \varepsilon\cos\theta+\ldots$ $\bar{s} = \mathrm{i}\sqrt{a\varepsilon\cos\theta}+\ldots$		$\bar{q} = Re^{i\psi}+\ldots$ $\bar{s} = \sqrt{aRe^{-i\psi}}+\ldots$			
	$\tan^{-1}\left(\frac{\bar{s}}{\sqrt{l_2^2-a^2}}\right) = O(1)+\ldots$		$\tan^{-1}\left(\frac{\bar{s}}{\sqrt{l_2^2-a^2}}\right) = \frac{\sqrt{Re^{-i\psi}}}{\sqrt{\varepsilon}}+\ldots$		$\tan^{-1}\left(\frac{\bar{s}}{\sqrt{l_2^2-a^2}}\right) = O(1)+\ldots$	

$$\bar{s}^2+l_2^2-a^2 = aRe^{-i\psi}+\ldots, \quad R > \varepsilon, \varepsilon \to 0 \tag{B30}$$

$$\bar{s}^2+l_2^2-a^2 = a\varepsilon+\ldots, \quad R < \varepsilon, \varepsilon \to 0. \tag{B31}$$

The latter expressions can be used in (Gradshteyn and Ryzhik, 1980):

$$\tan^{-1}\left(\frac{\bar{s}}{\sqrt{l_2^2-a^2}}\right) = \xi\left(1+\frac{\xi}{6}+\ldots\right), \tag{B32}$$

where

$$\xi = \frac{\bar{s}}{\sqrt{\bar{s}^2+l_2^2-a^2}}. \tag{B33}$$

Equations (B27), (B28), (B30), (B31) and (B33) yield:

$$\begin{aligned}
&\xi = 1+\ldots, \quad R > \varepsilon, \varepsilon \to 0\\
&\xi = \frac{\sqrt{Re^{-i\psi}}}{\sqrt{\varepsilon}}+\ldots, \quad \varepsilon\lvert\cos\theta\rvert < R < \varepsilon, \varepsilon \to 0\\
&\xi = \mathrm{i}\sqrt{\cos\theta}+\ldots, \quad R < \varepsilon\lvert\cos\theta\rvert, \varepsilon \to 0
\end{aligned} \tag{B34}$$

and hence

$$\begin{aligned}
&\tan^{-1}\left(\frac{\bar{s}}{\sqrt{l_2^2-a^2}}\right) = O(1)+\ldots, \quad R > \varepsilon, \quad \varepsilon \to 0\\
&\tan^{-1}\left(\frac{\bar{s}}{\sqrt{l_2^2-a^2}}\right) = \sqrt{\frac{Re^{-i\psi}}{\varepsilon}}+\ldots, \quad \varepsilon\lvert\cos\theta\rvert < R < \varepsilon, \quad \varepsilon \to 0\\
&\tan^{-1}\left(\frac{\bar{s}}{\sqrt{l_2^2-a^2}}\right) = O(1)+\ldots, \quad R < \varepsilon\lvert\cos\theta\rvert, \quad \varepsilon \to 0.
\end{aligned} \tag{B35}$$

The expansions made so far are collected in Table B1. Three intervals are to be considered:

Interval I: $R < \varepsilon\lvert\cos\theta\rvert$
Interval II: $\varepsilon\lvert\cos\theta\rvert < R < \varepsilon$
Interval III: $\varepsilon < R$.

Since, in order to find an expression for σ_3, σ_1 and σ_2 are to be determined [cf. eqns (A24) and (A25)], attention will be focused on $f_3(z)$ and $f_4(z)$.

Interval I. Substituting the above expansions into eqns (A9) and (A10) and (A58) and (A59) and taking the leading terms only yields:

$$f_{3,4}(z) = O\left(\frac{\sqrt{R}}{\varepsilon^3\sqrt{\varepsilon}}\right) + \ldots, \quad \varepsilon \to 0 \tag{B36}$$

$$f'_{3,4}(z) = O\left(\frac{\sqrt{R}}{\varepsilon^3\sqrt{\varepsilon}}\right) + \ldots, \quad \varepsilon \to 0 \tag{B37}$$

and hence

$$\sigma_1(z) = O\left(\frac{\sqrt{R}}{\varepsilon^2\sqrt{\varepsilon}}\right) + \ldots, \quad \varepsilon \to 0. \tag{B38}$$

Interval II. f_3 and f'_3 take the same form as in Interval I. However,

$$f_4(z) = O\left(\frac{1}{\sqrt{\varepsilon}\,R\sqrt{R}}\right) + O\left(\frac{\sqrt{R}}{\varepsilon^2\sqrt{\varepsilon}}\right) + \ldots, \quad \varepsilon \to 0 \tag{B39}$$

$$f'_4(z) = O\left(\frac{1}{\varepsilon\sqrt{\varepsilon}\,R\sqrt{R}}\right) + O\left(\frac{\sqrt{R}}{\varepsilon^3\sqrt{\varepsilon}}\right) + \ldots, \quad \varepsilon \to 0 \tag{B40}$$

and hence

$$\sigma_y(z) = O\left(\frac{1}{\sqrt{\varepsilon}\,R\sqrt{R}}\right) + O\left(\frac{\sqrt{R}}{\varepsilon^2\sqrt{\varepsilon}}\right) + \ldots, \quad \varepsilon \to 0. \tag{B41}$$

Interval III. Since Interval III is of great practical interest, the leading terms of the expansions will be given explicitly:

$$f_3(z) = \frac{1}{\sqrt{\varepsilon}} \frac{\sqrt{a^2-\rho_0^2}}{2R^2\sqrt{a}} \frac{\sqrt{1-\cos\theta}\,(1+\cos\theta)}{\sin\theta} + O(\sqrt{\varepsilon}), \quad \varepsilon \to 0 \tag{B42}$$

$$f_4(z) = -\frac{1}{\sqrt{\varepsilon}} \frac{\sqrt{a^2-\rho_0^2}}{2R^2\sqrt{a}} \frac{\sin\theta}{\sqrt{1-\cos\theta}} + \frac{\pi\sqrt{a^2-\rho_0^2}}{2R^2\sqrt{aR}} \left(\frac{\rho_0}{a} e^{i(\phi_0+(\psi/2))} - 2e^{-(3i\psi/2)}\right) + O(\sqrt{\varepsilon}), \quad \varepsilon \to 0 \tag{B43}$$

$$f'_3(z) = -\frac{1}{\varepsilon\sqrt{\varepsilon}} \frac{\sqrt{a^2-\rho_0^2}}{2R^2\sqrt{2a}} \sin\left(\frac{3\theta}{2}\right) + O\left(\frac{1}{\sqrt{\varepsilon}}\right), \quad \varepsilon \to 0 \tag{B44}$$

$$f'_4(z) = \frac{1}{\varepsilon\sqrt{\varepsilon}} \frac{\sqrt{a^2-\rho_0^2}}{2R^2\sqrt{2a}} \sin\left(\frac{3\theta}{2}\right) + O\left(\frac{1}{\sqrt{\varepsilon}}\right), \quad \varepsilon \to 0 \tag{B45}$$

and finally [cf. eqns (A49) and (A51)]

$$\sigma_1 = \frac{P}{\pi^2} \frac{\sqrt{a^2-\rho_0^2}}{R^2\sqrt{2a}} \frac{1}{\sqrt{\varepsilon}} \cos\left(\frac{\theta}{2}\right) \left\{1+2\nu-\sin\left(\frac{\theta}{2}\right)\sin\left(\frac{3\theta}{2}\right)\right\} + O(\sqrt{\varepsilon}), \quad \varepsilon \to 0 \tag{B46}$$

$$\sigma_2 = \frac{P}{\pi^2} \frac{\sqrt{a^2-\rho_0^2}}{R^2\sqrt{2a}} \frac{1}{\sqrt{\varepsilon}} \cos\left(\frac{\theta}{2}\right) \left\{1+2\nu-\sin\left(\frac{\theta}{2}\right)\sin\left(\frac{3\theta}{2}\right)\right\} - \frac{P(1-2\nu)\sqrt{a^2-\rho_0^2}}{2\pi R^2\sqrt{aR}} \left(\frac{\rho_0}{a} e^{i(\phi_0+(\psi/2))} - 2e^{-(3i\psi/2)}\right) + O(\sqrt{\varepsilon}), \quad \varepsilon \to 0 \tag{B47}$$

and

$$(\sigma_y)_1 \doteq \sigma_y = \frac{2P\nu}{\pi^2} \frac{\sqrt{a^2-\rho_0^2}}{R^2\sqrt{2a}} \frac{1}{\sqrt{\varepsilon}} \cos\left(\frac{\theta}{2}\right) + \frac{P(1-2\nu)\sqrt{a^2-\rho_0^2}}{4\pi R^2\sqrt{aR}} \left[\frac{\rho_0}{a}\cos\left(\phi_0+\frac{\psi}{2}\right) - 2\cos\left(\frac{3\psi}{2}\right)\right] + O(\sqrt{\varepsilon}), \quad \varepsilon \to 0. \tag{B48}$$

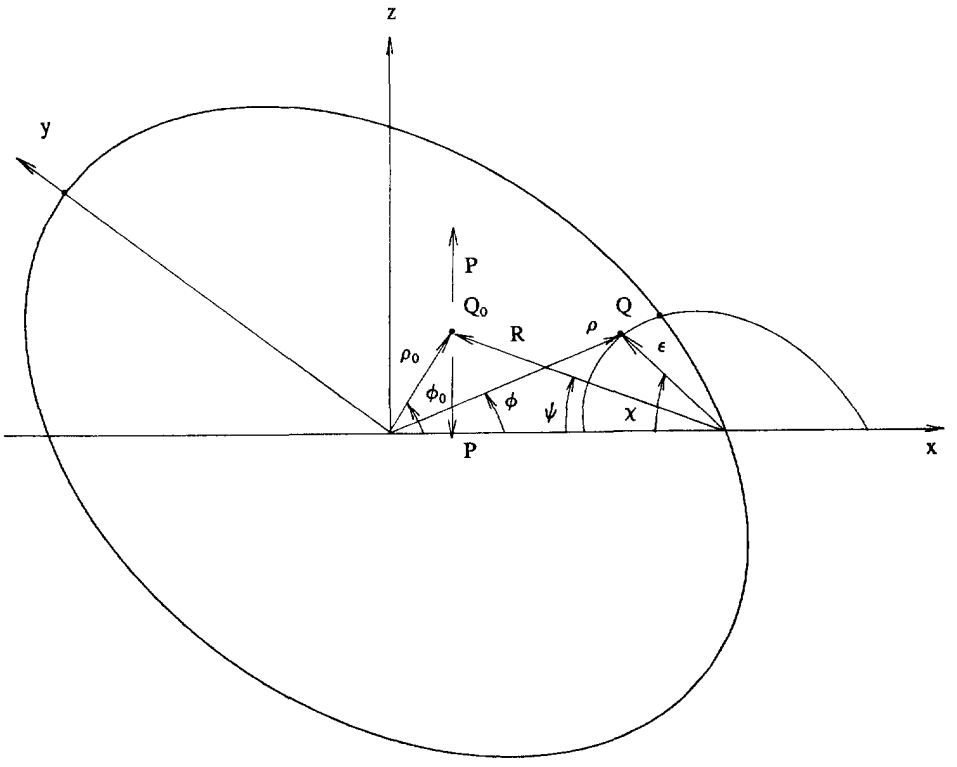

Fig. B2. Geometric parameters used for the determination of the asymptotic expansion of $(w)_1$.

This expression is valid for the whole range $-\pi \leqslant \theta \leqslant \pi$ because of symmetry conditions. In order to find $(\sigma_y)_1$ due to an arbitrary distributed load the above formulae have to be integrated over the appropriate ranges. For a constant distributed load p it can be shown that the integration over Interval III is dominant, leading to:

$$\sigma_y(p) = \int_{-\pi/2}^{\pi/2}\int_{\varepsilon}^{2a\cos\psi} p\frac{(\sigma_y)_1}{P} R\,\mathrm{d}R\,\mathrm{d}\psi \sim 2\nu\frac{p}{\pi^2\sqrt{2a}}\frac{1}{\sqrt{\varepsilon}}\cos\frac{\theta}{2}\int_{-\pi/2}^{\pi/2}\int_{\varepsilon}^{2a\cos\psi}\sqrt{\frac{2a\cos\psi - R}{R}}\,\mathrm{d}R\,\mathrm{d}\psi, \quad \varepsilon \to 0$$

$$\sim 2\nu\frac{p\sqrt{2a}}{\pi}\frac{1}{\sqrt{\varepsilon}}\cos\frac{\theta}{2}, \quad \varepsilon \to 0. \tag{B49}$$

This agrees with the findings of other authors [e.g. Fabrikant (1988)].

Displacement $(w)_1$

For the displacement function w, the attention is focused on a point Q belonging to the crack surface (Fig. B2) and described by either (ρ, ϕ, z) or (ε, χ, z) satisfying:

$$\rho\,\mathrm{e}^{\mathrm{i}\phi} = a - \varepsilon\,\mathrm{e}^{-\mathrm{i}\chi}, \quad \varepsilon \ll a, \quad -\pi/2 \leqslant \chi \leqslant \pi/2, \quad 0 \leqslant \varepsilon \leqslant 2a\cos\chi \tag{B50}$$

$$z = 0. \tag{B51}$$

For Q_0, eqn (B4) still applies. Since [cf. eqn (A55)]

$$w(z=0) = \frac{2HP}{\pi} f_2(z), \tag{B52}$$

only h and R_0 have to be examined. They take the form (cf. Appendix A):

$$R_0^2 = \varepsilon^2 + R^2 - 2\varepsilon R\cos(\chi - \psi) = (R - R_1^0)(R - R_2^0), \tag{B53}$$

where

$$R^0_{1,2} = \varepsilon e^{\pm i(\chi-\psi)}. \tag{B54}$$

Hence

$$|R^0_1| = |R^0_2| = \varepsilon. \tag{B55}$$

A Taylor expansion of eqn (B53) yields

$$R_0 = \varepsilon + \ldots, \quad R < \varepsilon \tag{B56}$$

$$R_0 = R + \ldots, \quad R > \varepsilon. \tag{B57}$$

Furthermore,

$$l_1 = \rho \tag{B58}$$

and

$$h = \frac{1}{a}\sqrt{\varepsilon(2a\cos\chi - \varepsilon)}\sqrt{R(2a\cos\psi - R)} \doteq B\sqrt{\varepsilon R}. \tag{B59}$$

Using eqn (B20), in which $(h^2 + R_0^2)$ now takes the form

$$h^2 + R_0^2 = (R - R'_1)(R - R'_2) + \ldots, \tag{B60}$$

where

$$R'_{1,2} = -\varepsilon e^{\pm i(\chi-\psi)}, \tag{B61}$$

one obtains for the leading behaviour of f_2 [cf. eqns (A8) and (B20)]:

$$f_2 = \frac{B\sqrt{R}}{\varepsilon\sqrt{\varepsilon}} + \ldots, \quad R < \varepsilon \tag{B62}$$

$$f_2 = \frac{B\sqrt{\varepsilon}}{R\sqrt{R}} + \ldots, \quad R > \varepsilon. \tag{B63}$$

Hence

$$(w)_1 \doteq w(z = O) = 0\left(\frac{\sqrt{R}}{\varepsilon\sqrt{\varepsilon}}\right) + \ldots, \quad R < \varepsilon \tag{B64}$$

$$(w)_1 \doteq w(z = 0) = \frac{2HP}{\pi}\frac{\sqrt{\varepsilon}}{R^2}\frac{\sqrt{2a\cos\chi}\sqrt{a^2 - \rho_0^2}}{a} + \ldots, \quad R > \varepsilon. \tag{B65}$$

Stress intensity factor

The stress intensity factor for a point load within a circular crack in infinite space was, for example, given by Gao and Rice (1987) and Fabrikant (1988). Here the formula given by Gao and Rice will be taken, since it corresponds to the usual definition of the stress intensity factor (Hahn, 1976; Tada, 1973). The formula given by Fabrikant is smaller by a factor of $(2\pi)^{1/2}$.

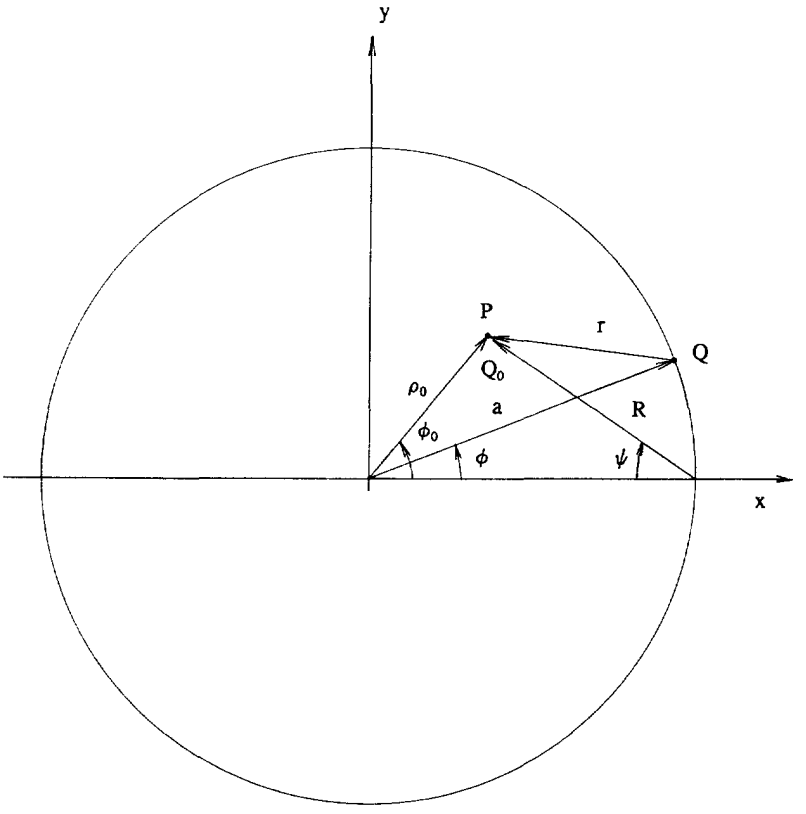

Fig. B3. Geometric parameters used for the determination of $K(\phi)$.

The stress intensity factor in a point on the crack front characterized by the angle ϕ, due to a point load at (ρ_0, ϕ_0) (Fig. B3) can be expressed as:

$$K(\phi) = \frac{P}{\pi\sqrt{\pi a}} \frac{\sqrt{a^2-\rho_0^2}}{r^2}, \tag{B66}$$

where

$$r^2 = a^2 + \rho_0^2 - 2a\rho_0 \cos(\phi - \phi_0). \tag{B67}$$

Since

$$\rho_0 \, e^{i\phi_0} = a - R\, e^{-i\psi}, \tag{B68}$$

eqn (B67) can be rewritten as:

$$r^2 = R^2 + 2aR[\cos(\phi+\psi) - \cos\psi] + 2a^2(1-\cos\phi). \tag{B69}$$

Since $r = 0$ can occur for $Q = Q_0$ only, the right hand side of eqn (B69) either has two complex conjugate roots, or one double root. Hence:

$$r^2 = (R-R_1)(R-R_2), \tag{B70}$$

where

$$|R_1| = |R_2| = a\sqrt{2(1-\cos\phi)}. \tag{B71}$$

The Taylor expansion of (B70) yields

$$r^2 = 2a^2(1-\cos\phi)+\ldots, \quad R < a\sqrt{2(1-\cos\phi)} \tag{B72}$$

$$r^2 = R^2+\ldots, \quad R > a\sqrt{2(1-\cos\phi)}. \tag{B73}$$

Hence

$$K(\phi) = \frac{P}{\pi\sqrt{\pi a}}\frac{\sqrt{a^2-\rho_0^2}}{2a^2(1-\cos\phi)}+\ldots, \quad R < a\sqrt{2(1-\cos\phi)} \tag{B74}$$

$$K(\phi) = \frac{P}{\pi\sqrt{\pi a}}\frac{\sqrt{a^2-\rho_0^2}}{R^2}+\ldots, \quad R > a\sqrt{2(1-\cos\phi)}. \tag{B75}$$

APPENDIX C: GREEN FUNCTIONS FOR A HALF INFINITE SPACE UNDER NORMAL LOADING ON THE FREE BOUNDARY

This well-known problem has been treated earlier, e.g. in cylindrical coordinates (Timoshenko and Goodier, 1970). Here it will be shown that the solution can be derived as a special case of the formulae in Appendix A by letting $a \to \infty$. The terminology is the same as in Fig. A1, in particular $z \geqslant 0$. For $a \to \infty$, eqns (A13)–(A17) take the form:

$$l_1 = \rho - \frac{\rho z^2}{2a^2} + O\left(\frac{1}{a^3}\right), \quad a \to \infty \tag{C1}$$

$$l_2 = a + \frac{z^2}{2a} + O\left(\frac{1}{a^3}\right), \quad a \to \infty \tag{C2}$$

$$L = a^2 + (z^2-\rho^2) + O\left(\frac{1}{a}\right), \quad a \to \infty \tag{C3}$$

$$R_0^2 = \rho^2 + \rho_0^2 - 2\rho\rho_0\cos(\phi-\phi_0) + z^2 \tag{C4}$$

$$h = a - \frac{1}{2}\frac{(\rho^2+\rho_0^2)}{a} + O\left(\frac{1}{a^3}\right), \quad a \to \infty \tag{C5}$$

$$\bar{q} = \rho e^{-i\phi} - \rho_0 e^{-i\phi_0} \tag{C6}$$

$$\bar{s} = a - \frac{\rho\rho_0}{2a}e^{i(\phi_0-\phi)} + O\left(\frac{1}{a^3}\right), \quad a \to \infty. \tag{C7}$$

The functions f_3, f_4, f_3' and f_4' yield:

$$f_3(z) \sim -\frac{\pi z}{2R_0^3}, \quad a \to \infty \tag{C8}$$

$$f_4(z) \sim -\frac{\pi}{\bar{q}^2} + \frac{\pi}{2}\frac{z(3R_0^2-z^2)}{\bar{q}R_0^3}, \quad a \to \infty \tag{C9}$$

$$f_3'(z) \sim -\frac{\pi}{2}\frac{(R_0^2-3z^2)}{R_0^5}, \quad a \to \infty \tag{C10}$$

$$f_4'(z) \sim \frac{\pi}{2}\frac{3(R_0^2-z^2)^2}{\bar{q}^2R_0^5}, \quad a \to \infty. \tag{C11}$$

Hence:

$$\sigma_1 \sim -\frac{zP}{2\pi R_0^3}\left[2(1+\nu)-\frac{3z^2}{R_0^2}\right], \quad a \to \infty \tag{C12}$$

$$\sigma_2 \sim \frac{P}{\pi\bar{q}^2}\left\{(1-2\nu)\left[1-\frac{z(3R_0^2-z^2)}{2R_0^3}\right]-\frac{3z(R_0^2-z^2)^2}{2R_0^5}\right\}, \quad a \to \infty. \tag{C13}$$

These formulae are in agreement with the literature (Timoshenko and Goodier, 1970).

APPENDIX D: STRESSES IN A HALF SPACE IN THE VICINITY OF A CRACK STRESS SINGULARITY LOADING ON THE FREE SURFACE

The stress singularity loading has the form [cf. eqn (B48)]:

$$\sigma_1 = (\sigma_y)_1 = \frac{K}{\sqrt{\rho_1}}\cos\left(\frac{\phi_1}{2}\right), \tag{D1}$$

where

$$K = 2\nu\frac{P}{\pi^2}\frac{\sqrt{a^2-\rho_0^2}}{R^2\sqrt{2a}}. \tag{D2}$$

The two variables ε and θ in eqn (B48) have been replaced by ρ_1 and ϕ_1 (Fig. D1). The point force corresponding to an infinitesimal surface element in Q_0 is

$$\mathrm{d}P = \sigma_y \rho_1 \,\mathrm{d}\rho_1 \,\mathrm{d}\phi_1. \tag{D3}$$

The stress singularity is positioned in the origin. An arbitrary point inside the half space is characterized by (ρ, ϕ, z). A point in the vicinity of the singularity in a plane perpendicular to the free surface and containing the x-axis can be described by the three parameters ε, θ_1 and $\phi = 0, \pi$. The following relationships exist:

$$z = \varepsilon\sin\theta_1, \quad \rho\,\mathrm{e}^{-i\psi} = \varepsilon\cos\theta_1, \quad 0 \leqslant \theta_1 \leqslant \pi \tag{D4}$$

and [eqns (C4) and (C6)]:

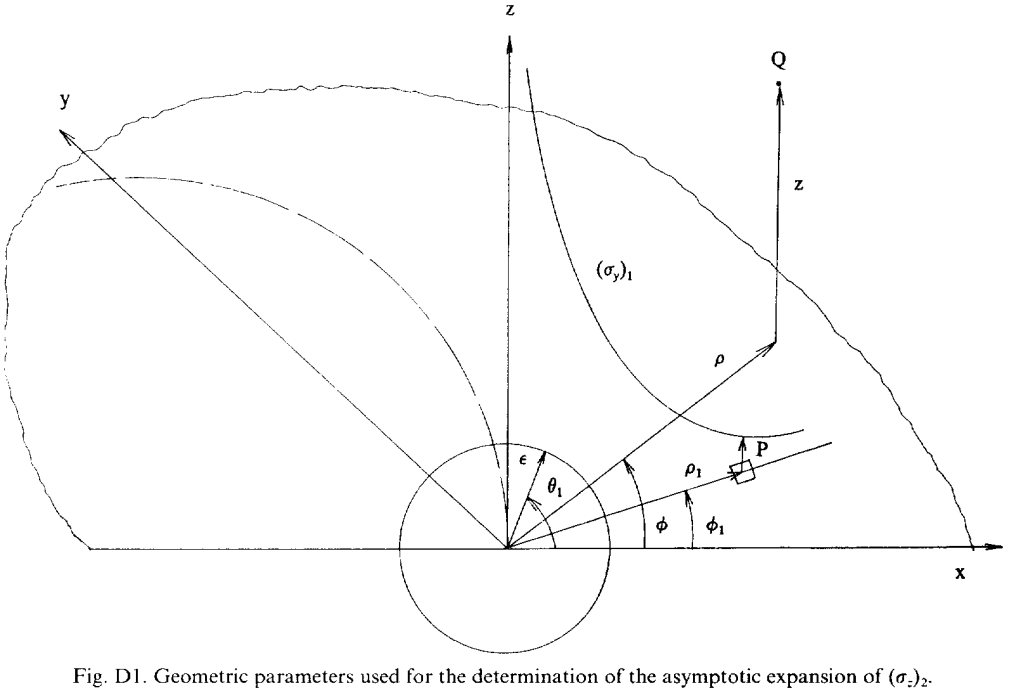

Fig. D1. Geometric parameters used for the determination of the asymptotic expansion of $(\sigma_z)_2$.

$$\bar{q} = \varepsilon \cos\theta_1 - \rho_1 e^{-i\phi_1} \tag{D5}$$

$$R_0^2 = \varepsilon^2 + \rho_1^2 - 2\rho_1 \varepsilon \cos\theta_1 \cos\phi_1 \doteq R_1^2. \tag{D6}$$

Substituting these relationships into eqns (C12) and (C13) yields:

$$d\sigma_1 = -\frac{\varepsilon \sin\theta_1}{R_1^3} \frac{K\sqrt{\rho_1}\cos\left(\frac{\phi_1}{2}\right)}{2\pi} d\rho_1\, d\phi_1 \left\{2(1+\nu) - \frac{3\varepsilon^2 \sin^2\theta_1}{R_1^2}\right\} \tag{D7}$$

$$d\sigma_2 = -\frac{K\sqrt{\rho_1}\cos\left(\frac{\phi_1}{2}\right)}{2\pi\bar{q}^2 R_1^3} d\rho_1\, d\phi_1 \cdot \left\{(1-2\nu)[-2R_1^3 + \varepsilon \sin\theta_1 (3R_1^2 - \varepsilon^2 \sin^2\theta_1)] + \frac{3\varepsilon \sin\theta_1 (R_1^2 - \varepsilon^2 \sin^2\theta_1)^2}{R_1^2}\right\}. \tag{D8}$$

σ_1 and σ_2 are obtained by integration:

$$\sigma_{1,2} = \int_{-\pi}^{\pi} \int_0^{\eta} d\sigma_{1,2}, \tag{D9}$$

where $0 < \eta \leqslant R$. R is defined in Fig. B1 and is the limit of the domain of validity of eqn (B48). Equations (D7)–(D9) yield ($\rho_1 = x\varepsilon$):

$$\sigma_1 = -\frac{K \sin\theta_1}{\pi\sqrt{\varepsilon}} \int_0^{\pi} \cos\left(\frac{\phi_1}{2}\right) \int_0^{\eta/\varepsilon} \left\{2(1+\nu) - \frac{3\sin^2\theta_1}{\alpha^2}\right\} \frac{\sqrt{x}}{\alpha^3} dx\, d\phi_1 \tag{D10}$$

$$\sigma_2 = \frac{K}{\pi\sqrt{\varepsilon}} \int_{-\pi}^{\pi} \cos\left(\frac{\phi_1}{2}\right) \int_0^{\eta/\varepsilon} \left\{(1-2\nu) - 3(1-\nu)\frac{\sin\theta_1}{\alpha} + \frac{(7-2\nu)}{2}\frac{\sin^2\theta_1}{\alpha^2} - \frac{3}{2}\frac{\sin^5\theta_1}{\alpha^5}\right\} \frac{\sqrt{x}}{\beta^2} dx\, d\phi_1, \tag{D11}$$

where

$$\alpha = \sqrt{1 + x^2 - 2x\cos\theta_1 \cos\phi_1} \tag{D12}$$

$$\beta = \cos\theta_1 - x e^{-i\phi_1}. \tag{D13}$$

Since the imaginary part of the integrand of σ_2 is antisymmetric in ϕ_1, σ_2 is real. In eqns (D10) and (D11), η/ε can be replaced by ∞. Indeed, since

$$\alpha \sim x, \quad x \to \infty \tag{D14}$$

$$\beta \sim -x e^{-i\phi_1}, \quad x \to \infty, \tag{D15}$$

the error made amounts to

$$\Delta\sigma_1 \sim -\frac{2K \sin\theta_1 (1+\nu)}{\pi\sqrt{\varepsilon}} \int_0^{\pi} \cos\left(\frac{\phi_1}{2}\right) \int_{\eta/\varepsilon}^{\infty} \frac{dx\, d\phi_1}{x^2\sqrt{x}} = O(\varepsilon), \quad \varepsilon \to 0 \tag{D16}$$

and

$$\Delta\sigma_2 \sim \frac{K(1-2\nu)}{\pi\sqrt{\varepsilon}} \int_{-\pi}^{\pi} \cos\left(\frac{\phi_1}{2}\right) e^{2i\phi_1} \int_{\eta/\varepsilon}^{\infty} \frac{dx\, d\phi_1}{x\sqrt{x}} = O(1), \quad \varepsilon \to 0, \tag{D17}$$

which is subdominant with respect to the $\varepsilon^{-1/2}$ behaviour emerging from the 0 to ∞ integration for σ_1 and σ_2.

Since the crack surface (dashed line in Fig. D1) is of main interest, the following discussion will be limited to $\pi/2 \leqslant \theta_1 \leqslant \pi$. In order to evaluate σ_1 and σ_2 numerically it is important to know whether the integrands have any singularities. To this end the zeros of α and β are examined.

Defining new coordinates (δ, ψ) by

$$\delta e^{-i\psi} \doteq -\beta \tag{D18}$$

or

$$x\cos\phi_1 = \cos\theta_1 + \delta\cos\psi \tag{D19}$$

$$x\sin\phi_1 = \delta\sin\psi, \tag{D20}$$

the following relations can be established:

$$x = \sqrt{\cos^2\theta_1 + 2\delta\cos\theta_1\cos\psi + \delta^2} \tag{D21}$$

and

$$\sqrt{x}\cos\frac{\phi_1}{2} = \sqrt{\frac{x + x\cos\phi_1}{2}}. \tag{D22}$$

Substitution of eqns (D19) and (D21) into eqn (D22) yields:

$$\sqrt{x}\cos\frac{\phi_1}{2} = \frac{\delta|\sin\psi|}{2\sqrt{|\cos\theta_1|}}\left[1 - \frac{\delta\cos\psi}{2\cos\theta_1} + O(\delta^2)\right], \quad \delta \to 0, \theta_1 \neq \pi/2. \tag{D23}$$

Furthermore,

$$\alpha^2 = \sin^2\theta_1 + \delta^2 \tag{D24}$$

and hence

$$\alpha^n = \sin^n\theta_1\left\{1 + \frac{n\delta^2}{2}\frac{1}{\sin^2\theta_1} + O(\delta^4)\right\}, \quad \delta \to 0, \quad \theta_1 \neq 0, \pi. \tag{D25}$$

From eqn (D24) it is clear that $\alpha = 0$ only for $\theta_1 = \pi$ and $\delta = 0$ ($\theta_1 = 0$ was excluded). This case will be treated separately.

For $\theta_1 \neq 0, \pi$ the integrand of σ_1 does not contain any poles and the integral converges. A typical term of the integrand of σ_2 is:

$$g_n(x, \phi_1) \doteq \frac{\cos(\phi_1/2)\sqrt{x}}{\alpha^n\beta^2}. \tag{D26}$$

Substitution of eqns (D18), (D23) and (D25) yields:

$$g_n(x, \phi_1) = \frac{|\sin\psi|}{2\delta\sqrt{|\cos\theta_1|}}\frac{e^{2i\psi}}{\sin^n\theta_1}\left[1 - \frac{\delta\cos\psi}{2\cos\theta_1} + O(\delta^2)\right], \quad \delta \to 0. \tag{D27}$$

Defining

$$h(n) \doteq \frac{|\sin\psi|}{2\delta\sqrt{|\cos\theta_1|}}\frac{e^{2i\psi}}{\sin^n\theta_1}\left[1 - \frac{\delta\cos\psi}{2\cos\theta_1}\right], \tag{D28}$$

it is easy to check that

$$2(1-2\nu)\cdot h(0) - 6(1-\nu)\sin\theta_1\cdot h(1) + (7-2\nu)\sin^3\theta_1\cdot h(3) - 3\sin^5\theta_1\cdot h(5) = 0, \tag{D29}$$

which means that the integrand of σ_2 in eqn (D11), which will be denoted by $I(\sigma_2)$, satisfies

$$I(\sigma_2) = o(1), \quad \delta \to 0. \tag{D30}$$

Changing the integration variables from (x, ϕ_1) to (δ, ψ) yields:

$$\sigma_2 = \int_{\phi_1=-\pi}^{\pi}\int_{x=0}^{\infty}\frac{I(\sigma_2)}{x}x\,\mathrm{d}x\,\mathrm{d}\phi_1 = \int_{\psi=-\pi}^{\pi}\int_{\delta=0}^{\infty}\frac{I(\sigma_2)}{x}\delta\,\mathrm{d}\delta\,\mathrm{d}\psi \doteq \int_{\psi=-\pi}^{\pi}\int_{\delta=0}^{\infty} I'(\sigma_2)\,\mathrm{d}\delta\,\mathrm{d}\psi, \tag{D31}$$

where

$$I'(\sigma_2) = \frac{I(\sigma_2)\delta}{\sqrt{\cos^2\theta_1 + 2\delta\cos\theta_1\cos\psi + \delta^2}}. \tag{D32}$$

Hence

$$I'(\sigma_2) = o(\delta), \quad \delta \to 0, \tag{D33}$$

which is clearly integrable.

Two special cases are considered. If $\theta_1 = \pi/2$, eqn (D23) is no longer valid. Deriving all expressions anew, one gets:

$$x = \delta \tag{D34}$$

$$\phi_1 = \psi \tag{D35}$$

$$\sqrt{x}\cos\frac{\phi_1}{2} = \sqrt{\delta}\cos\frac{\psi}{2} \tag{D36}$$

$$\alpha'' = 1 + \frac{n\delta^2}{2} + O(\delta^4), \quad \delta \to 0 \tag{D37}$$

$$g_n(x,\phi_1) = \frac{\sqrt{\delta}\cos\left(\dfrac{\psi}{2}\right)e^{2i\psi}}{\delta^2}\left[1 - \frac{n\delta^2}{2} + O(\delta^4)\right], \quad \delta \to 0 \tag{D38}$$

$$I'(\sigma_2) = I(\sigma_2) = o(\sqrt{\delta}), \quad \delta \to 0. \tag{D39}$$

If $\theta_1 = \pi$, then

$$\sigma_1 = 0 \tag{D40}$$

and

$$I(\sigma_2) \sim \frac{\cos(\phi_1/2)\sqrt{x}}{\beta^2} \sim \frac{\delta|\sin\psi|}{2}\frac{e^{2i\psi}}{\delta^2} \sim \frac{|\sin\psi|}{2\delta}e^{2i\psi}, \quad \delta \to 0. \tag{D41}$$

Hence

$$I'(\sigma_2) \sim \frac{|\sin\psi|}{2}e^{2i\psi}, \quad \delta \to 0 = O(1), \tag{D42}$$

which is clearly integrable. This concludes the proof that the integrands of σ_1 and σ_2 do not have any poles. Consequently the integrals in eqns (D10) and (D11) are regular for $\pi/2 \leqslant \theta_1 \leqslant \pi$. The stresses σ_x and σ_y can be evaluated using eqns (A24) and (A25). σ_1 takes the form:

$$(\sigma_z)_2 \doteq \sigma_1 = \frac{Kf(\theta_1)}{\sqrt{\varepsilon}}, \tag{D43}$$

where

$$f(\theta_1) = -\frac{1}{2}\int_0^{\pi}\cos\frac{\phi_1}{2}\int_0^{\infty}\left\{\frac{2(1+\nu)\sin\theta_1}{\pi} - \frac{3\sin^3\theta_1}{\pi\alpha^2}\right\}\frac{\sqrt{x}}{\alpha^3}\mathrm{d}x\,\mathrm{d}\phi_1$$
$$-\frac{1}{2\pi}\int_{-\pi}^{\pi}\cos\frac{\phi_1}{2}\int_0^{\infty}\left\{(1-2\nu) - \frac{3(1-\nu)\sin\theta_1}{\alpha} + \frac{(7-2\nu)\sin^3\theta_1}{2\alpha^3} - \frac{3\sin^5\theta_1}{2\alpha^5}\right\}\frac{\sqrt{x}}{\beta^2}\mathrm{d}x\,\mathrm{d}\phi_1. \tag{D44}$$

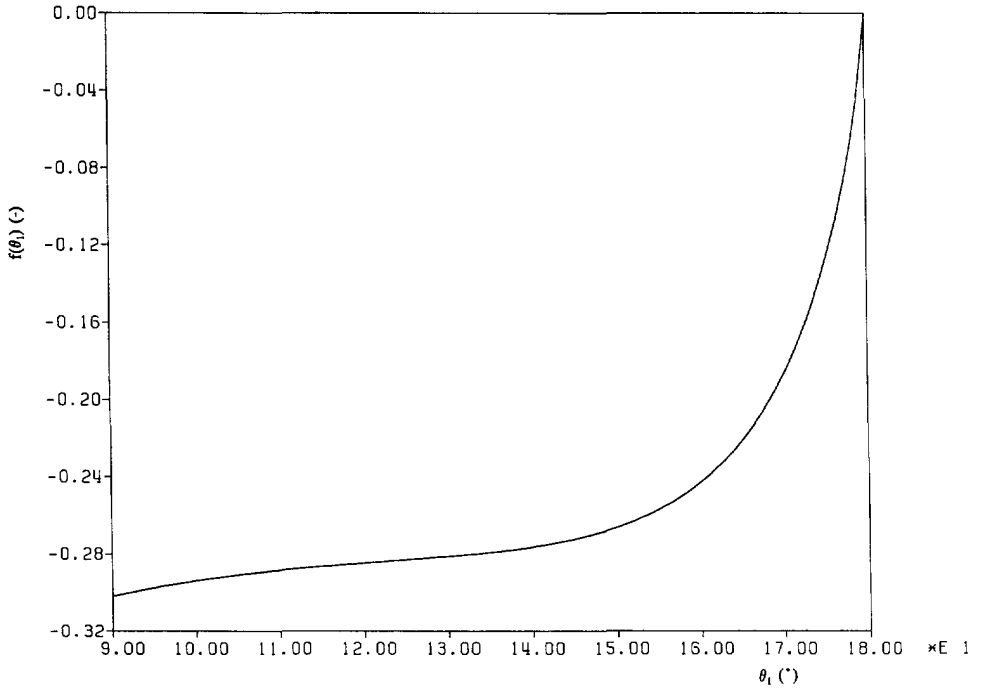

Fig. D2. Function $f(\theta_1)$.

$f(\theta_1)$ is shown for $\nu = 0.3$ in Fig. D2 and corresponds very well with the polynomial expression given by Hartranft and Sih (1973). Note that $f(\theta_1)$ is a linear function of ν.

APPENDIX E: STRESSES, DISPLACEMENTS AND STRESS INTENSITY FACTOR IN INFINITE SPACE DUE TO A CRACK LOADING BY THE LEADING BEHAVIOUR OF $(\sigma_z)_2$

Normal stress $(\sigma_y)_3$

The problem is sketched in Fig. E1. The load on an infinitesimal surface element $R\,\mathrm{d}R\,\mathrm{d}\psi$ can be expressed as [eqn. (D43)]:

$$\mathrm{d}P = (\sigma_z)_2 R\,\mathrm{d}R\,\mathrm{d}\psi = \frac{Kf(\pi-\psi)\,R\,\mathrm{d}R\,\mathrm{d}\psi}{\sqrt{R}}. \tag{E1}$$

In Appendix B it is shown that the effect of $\mathrm{d}P$ depends on the relative size of R with respect to ε. For the stress $(\sigma_y)_3$ one can write [cf. eqns (B38), (B41) and (B48); Fig. E2]:

$$\begin{aligned}(\sigma_y)_3 = &\iint_{\mathrm{Ia}+\mathrm{Ib}} \left[O\left(\frac{\sqrt{R}}{\varepsilon^2\sqrt{\varepsilon}}\right)+\dots\right] Kf(\pi-\psi)\sqrt{R}\,\mathrm{d}R\,\mathrm{d}\psi \\ &+ \iint_{\mathrm{IIa}+\mathrm{IIb}} \left[O\left(\frac{1}{\sqrt{\varepsilon}R\sqrt{R}}\right)+O\left(\frac{\sqrt{R}}{\varepsilon^2\sqrt{\varepsilon}}\right)+\dots\right] Kf(\pi-\psi)\sqrt{R}\,\mathrm{d}R\,\mathrm{d}\psi \\ &+ \iint_{\mathrm{III}} \frac{2\nu}{\pi^2}\frac{\sqrt{a^2-\rho_0^2}}{R^2\sqrt{2a}}\frac{1}{\sqrt{\varepsilon}}\cos\frac{\theta}{2} Kf(\pi-\psi)\sqrt{R}\,\mathrm{d}R\,\mathrm{d}\psi. \end{aligned} \tag{E2}$$

Looking at the different zones in detail:

Zone Ia

$$2\int_0^{\psi_1}\int_0^{\varepsilon|\cos\theta|}\left[O\left(\frac{\sqrt{R}}{\varepsilon^2\sqrt{\varepsilon}}\right)+\dots\right] Kf(\pi-\psi)\sqrt{R}\,\mathrm{d}R\,\mathrm{d}\psi = O\left(\frac{1}{\sqrt{\varepsilon}}\right)+\dots \tag{E3}$$

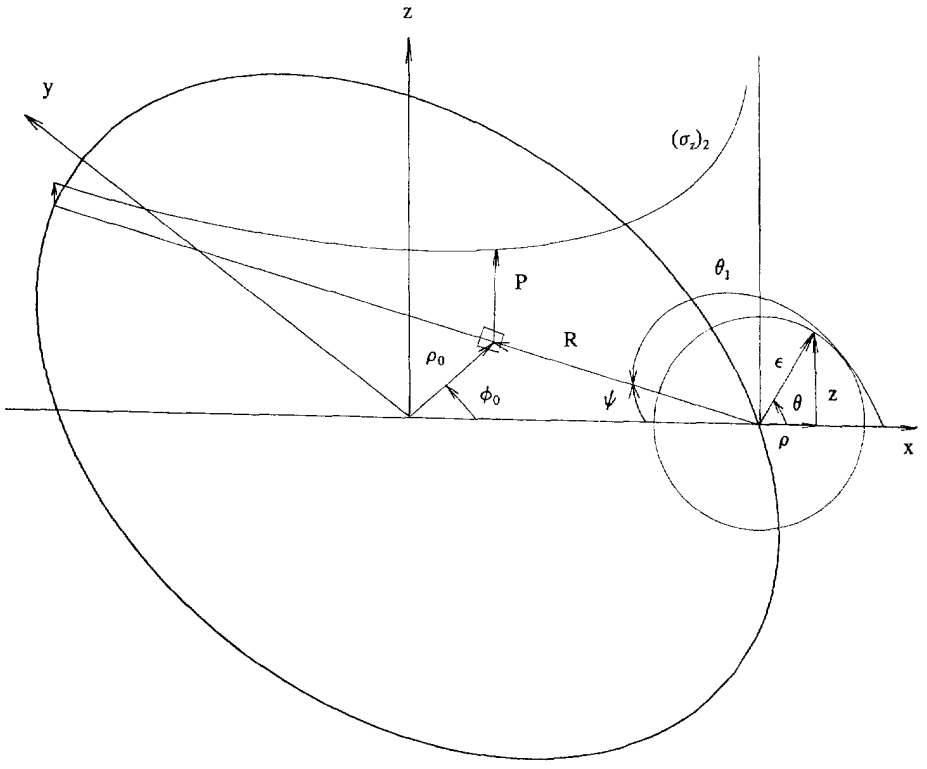

Fig. E1. Geometric parameters used for the determination of the asymptotic expansion of $(\sigma_z)_3$.

Zone Ib

$$2\int_{\psi_1}^{\pi/2}\int_0^{2a\cos\psi}\left[O\left(\frac{\sqrt{R}}{\varepsilon^2\sqrt{\varepsilon}}\right)+\dots\right]Kf(\pi-\psi)\sqrt{R}\,\mathrm{d}R\,\mathrm{d}\psi=\int_{\psi}^{\pi/2}\left[O\left(\frac{\cos^2\psi}{\varepsilon^2\sqrt{\varepsilon}}\right)+\dots\right]\mathrm{d}\psi. \tag{E4}$$

Furthermore,

$$\psi_1\sim\frac{\pi}{2}-\frac{\varepsilon|\cos\theta|}{2a},\quad \varepsilon\to 0 \tag{E5}$$

$$\cos\psi\sim\frac{\pi}{2}-\psi,\quad \varepsilon\to 0. \tag{E6}$$

Hence, eqn (E4) amounts to:

$$\int_{(\pi/2)-(\varepsilon|\cos\theta|/2a)}^{\pi/2}\left[O\left(\frac{(\pi/2-\psi)^2}{\varepsilon^2\sqrt{\varepsilon}}\right)+\dots\right]\mathrm{d}\psi=O(\sqrt{\varepsilon})+\dots,\quad \varepsilon\to 0. \tag{E7}$$

Zone IIa

$$2\int_0^{\psi_2}\int_{\varepsilon|\cos\theta|}^{\varepsilon}\left[O\left(\frac{1}{\sqrt{\varepsilon}\,R\sqrt{R}}\right)+O\left(\frac{\sqrt{R}}{\varepsilon^2\sqrt{\varepsilon}}\right)+\dots\right]Kf(\pi-\psi)\sqrt{R}\,\mathrm{d}R\,\mathrm{d}\psi$$
$$=2\int_0^{\psi_2}\left[O\left(\frac{\ln(R)}{\sqrt{\varepsilon}}\right)+O\left(\frac{1}{\sqrt{\varepsilon}}\right)+\dots\right]_{\varepsilon|\cos\theta|}^{\varepsilon}\mathrm{d}\psi=O\left(\frac{1}{\sqrt{\varepsilon}}\right)+\dots,\quad \varepsilon\to 0. \tag{E8}$$

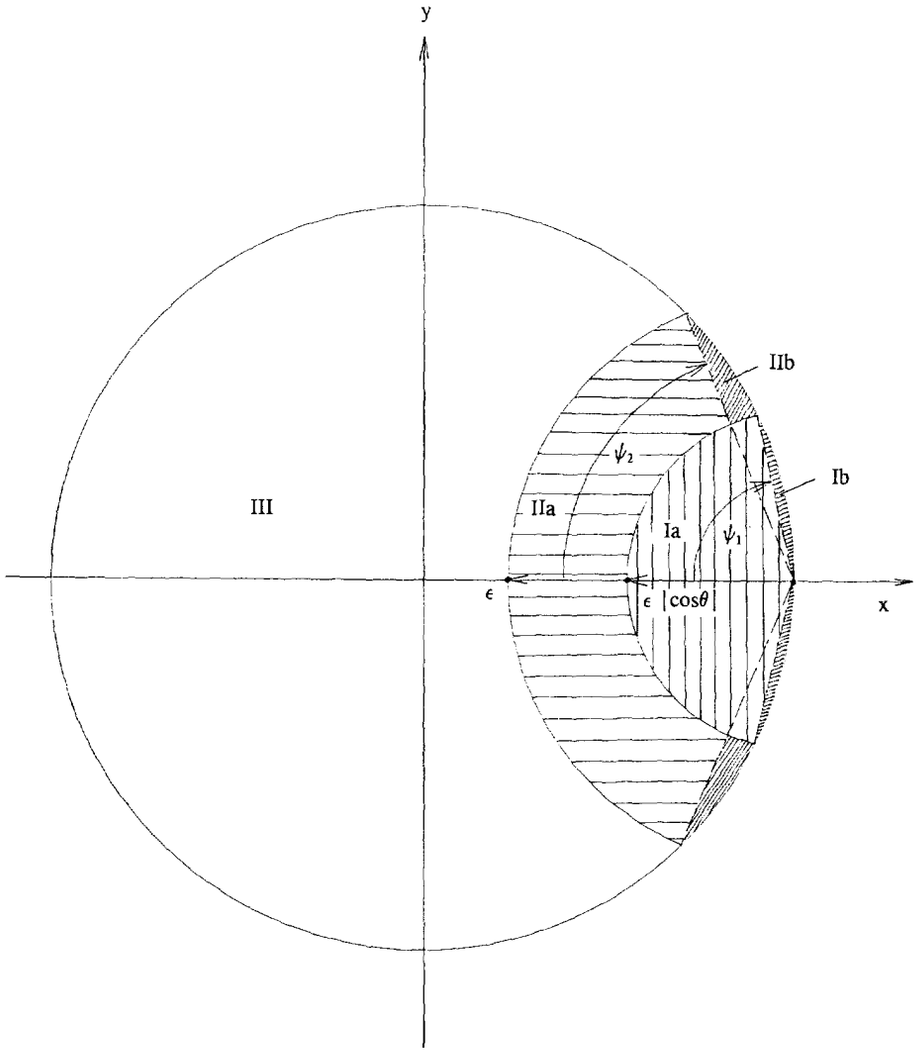

Fig. E2. The different integration domains for the determination of $(\sigma_1)_3$.

Zone IIb

$$2\int_{\psi_2}^{\psi_1}\int_{\varepsilon|\cos\theta|}^{2a\cos\psi}\left[O\left(\frac{1}{\sqrt{\varepsilon}\,R\sqrt{R}}\right)+O\left(\frac{\sqrt{R}}{\varepsilon^2\sqrt{\varepsilon}}\right)+\ldots\right]Kf(\pi-\psi)\sqrt{R}\,\mathrm{d}R\,\mathrm{d}\psi$$

$$=2\int_{\psi_2}^{\psi_1}\left[O\left(\frac{\ln\dfrac{2a\cos\psi}{\varepsilon|\cos\theta|}}{\sqrt{\varepsilon}}\right)+O\left(\frac{4a^2\cos^2\psi-\varepsilon^2\cos^2\theta}{\varepsilon^2\sqrt{\varepsilon}}\right)+\ldots\right]\mathrm{d}\psi,\quad \varepsilon\to 0. \tag{E9}$$

Furthermore, eqns (E5) and (E6) are still valid and

$$\psi_2\sim\frac{\pi}{2}-\frac{\varepsilon}{2a},\quad \varepsilon\to 0. \tag{E10}$$

Hence eqn (E9) amounts to:

$$O(\sqrt{\varepsilon}\ln\varepsilon)+\ldots,\quad \varepsilon\to 0. \tag{E11}$$

Zone III

The integral to be examined is:

$$\frac{4\nu K}{\pi^2\sqrt{2a}}\frac{\cos\frac{\theta}{2}}{\sqrt{\varepsilon}}\int_0^{\pi/2} f(\pi-\psi)\int_\varepsilon^{2a\cos\psi}\frac{\sqrt{2a\cos\psi-R}}{R}\,\mathrm{d}R\,\mathrm{d}\psi. \tag{E12}$$

Since

$$\int_\varepsilon^{2a\cos\psi}\frac{\sqrt{2a\cos\psi-R}}{R}\,\mathrm{d}R$$

$$= -2\sqrt{2a\cos\psi-\varepsilon}+\sqrt{2a\cos\psi}\,\ln\left\{\frac{4a\cos\psi-\varepsilon+2\sqrt{2a\cos\psi(2a\cos\psi-\varepsilon)}}{\varepsilon}\right\}$$

$$\sim -\sqrt{2a\cos\psi}\,\ln\varepsilon,\quad \varepsilon\to 0, \tag{E13}$$

eqn (E12) can be written as:

$$-\frac{4\nu K}{\pi^2}\cos\frac{\theta}{2}\frac{\ln\varepsilon}{\sqrt{\varepsilon}}\int_0^{\pi/2} f(\pi-\psi)\sqrt{\cos\psi}\,\mathrm{d}\psi+O\left(\frac{1}{\sqrt{\varepsilon}}\right),\quad \varepsilon\to 0, \tag{E14}$$

where

$$-\int_0^{\pi/2} f(\pi-\psi)\sqrt{\cos\psi}\,\mathrm{d}\psi = 0.1788+0.3856\nu \doteq F(\nu). \tag{E15}$$

Collecting all terms it is clear that zone III is dominant. Hence the important result:

$$(\sigma_\iota)_3 = \frac{4\nu K}{\pi^2}\cos\frac{\theta}{2}\frac{\ln\varepsilon}{\sqrt{\varepsilon}}F(\nu)+O\left(\frac{1}{\sqrt{\varepsilon}}\right),\quad \varepsilon\to 0. \tag{E16}$$

Displacement $(\mathrm{w})_3$

A similar analysis to the one in the previous section can be applied to $w\,(z=0)$ using eqns (B64) and (B65). Now there are only two zones. The result is:

$$w\sim\frac{8HK}{\pi}\sqrt{\cos\chi}\,\sqrt{\varepsilon}\ln\varepsilon\,F(\nu),\quad \varepsilon\to 0. \tag{E17}$$

The meaning of χ and ε is illustrated in Fig. B2.

The stress intensity factor

Equations (B74) and (B75) give the stress intensity factor due to a point load. They indicate that the integration over R will have to be split into three contributions (two zones):

$$K(\phi)_\iota = \frac{2K}{\sqrt{a\pi}\sqrt{\pi}}\left\{\frac{1}{2a^2(1-\cos\phi)}\int_0^{\psi_1} f(\pi-\psi)\int_0^{a\sqrt{2(1-\cos\phi)}} R\sqrt{2a\cos\psi-R}\,\mathrm{d}R\,\mathrm{d}\psi\right.$$

$$+\frac{1}{2a^2(1-\cos\phi)}\int_{\psi_1}^{\pi/2} f(\pi-\psi)\int_0^{2a\cos\psi} R\sqrt{2a\cos\psi-R}\,\mathrm{d}R\,\mathrm{d}\psi$$

$$\left.+\int_0^{\psi_1} f(\pi-\psi)\int_{a\sqrt{2(1-\cos\phi)}}^{2a\cos\psi}\frac{\sqrt{2a\cos\psi-R}}{R}\,\mathrm{d}R\,\mathrm{d}\psi\right\}, \tag{E18}$$

where

$$\psi_1 = \cos^{-1}\sqrt{\frac{1-\cos\phi}{2}} = \frac{\pi}{2}-\frac{\phi}{2}. \tag{E19}$$

The inner integral in the first term can be written as

$$\int_0^{a\sqrt{2(1-\cos\phi)}} R\sqrt{2a\cos\psi - R}\,\mathrm{d}R = \sqrt{2a\cos\psi}\,a^2(1-\cos\phi)+\ldots \tag{E20}$$

and consequently the first term is of $O(1)$, $\phi \to 0$.

The inner integral of the second term amounts to

$$\int_0^{2a\cos\psi} R\sqrt{2a\cos\psi - R}\,\mathrm{d}R \sim 2a^2\sqrt{2a}\cos^{5/2}\psi \sim 2a^2\sqrt{2a}\left(\frac{\pi}{2}-\psi\right)^{5/2}, \quad \phi \to 0. \tag{E21}$$

Since

$$\frac{\pi}{2} - \psi_1 = \frac{\phi}{2}, \tag{E22}$$

the second term is asymptotically equal to

$$\frac{1}{a^2\phi^2} f\left(\frac{\pi}{2}\right) \int_{\frac{\pi}{2}-\frac{\psi}{2}}^{\pi/2} 2a^2\sqrt{2a}\left(\frac{\pi}{2}-\psi\right)^{5/2} \mathrm{d}\psi = O(\phi^{3/2}), \quad \phi \to 0. \tag{E23}$$

The third term inside the parentheses is asymptotically equal to

$$-\ln\left(a\sqrt{2(1-\cos\phi)}\right) \int_0^{\pi/2} f(\pi-\psi)\sqrt{2a\cos\psi}\,\mathrm{d}\psi \sim \sqrt{2a}\,F(\nu)\ln\phi, \quad \phi \to 0. \tag{E24}$$

Hence

$$K(\phi)_1 \sim \frac{2\sqrt{2}K}{\pi\sqrt{\pi}} F(\nu)\ln\phi, \quad \phi \to 0. \tag{E25}$$

Conclusions

In all previous sections the effect of the outer integral was dominant. If for some reason the loading on the domain of the inner integrals is reduced in absolute value, this will not influence the dominant behaviour.

APPENDIX F: STRESSES IN A HALF INFINITE SPACE DUE TO A LOADING ON THE FREE BOUNDARY BY $(\sigma_r)_2$

The normal loading is taken from eqn (E16):

$$(\sigma_r)_2 = \frac{4\nu K}{\pi^2}\cos\frac{\theta}{2}\frac{\ln\varepsilon}{\sqrt{\varepsilon}}F(\nu), \quad \varepsilon \to 0 \tag{F1}$$

or, taking the notation of Appendix D (Fig. D1):

$$\sigma_r = L\frac{\ln\rho_2}{\sqrt{\rho_1}}\cos\frac{\phi_1}{2}. \tag{F2}$$

where

$$L = \frac{4\nu K}{\pi^2}F(\nu). \tag{F3}$$

Using the same approach as in Appendix D, σ_1 takes the following form:

$$\sigma_1 = -\frac{L\sin\theta_1}{\pi\sqrt{\varepsilon}}\left\{2(1+\nu)\int_0^{\pi}\cos\left(\frac{\phi_1}{2}\right)\int_0^{\eta_1}\frac{\sqrt{x}\ln(\varepsilon x)\,\mathrm{d}x}{[1+x^2-2x\cos\theta_1\cos\phi_1]^{3/2}}\mathrm{d}\phi_1 - 3\sin^2\theta_1\int_0^{\pi}\cos\left(\frac{\phi_1}{2}\right)\int_0^{\eta_1 x}\frac{\sqrt{x}\ln(\varepsilon x)\,\mathrm{d}x}{[1+x^2-2x\cos\theta_1\cos\phi_1]^{5/2}}\mathrm{d}\phi_1\right\}, \tag{F4}$$

where η is a measure of the domain in which eqn (E1) can be considered to be a good approximation. The first question which arises is whether η/ε in eqn (F4) can be replaced by ∞ without changing the leading behaviour. The error amounts to

$$\Delta\sigma_1 = \int_{\eta/\varepsilon}^{\infty} \frac{\sqrt{x}\ln(\varepsilon x)\,\mathrm{d}x}{[1+x^2-2x\cos\theta_1\cos\phi_1]^{n/2}}, \quad n = 3 \vee 5 \tag{F5}$$

$$\sim \int_{\eta/\varepsilon}^{\infty} \frac{\ln(\varepsilon x)}{x^{n-1/2}}\,\mathrm{d}x, \quad \varepsilon \to 0 \tag{F6}$$

$$\sim \frac{x^{3/2-n}}{(3/2-n)}\left\{\ln(\varepsilon x) - \frac{1}{(3/2-n)}\right\}\Bigg|_{\eta/\varepsilon}^{\infty}, \quad \varepsilon \to 0, \quad n > 3/2 \tag{F7}$$

$$\sim \varepsilon^{n-3/2}, \quad \varepsilon \to 0, \quad n > 3/2. \tag{F8}$$

For the integrands in eqn (F4) this amounts to $O(\varepsilon^{3/2})$ and $O(\varepsilon^{7/2})$, which is clearly subdominant compared to the $\ln\varepsilon$ leading behaviour of the integrals from 0 to ∞. Consequently, η/ε can be replaced by ∞. The same argument applies to σ_2. Similar to eqn (D43), one arrives at

$$(\sigma_z)_4 = Lf(\theta_1)\frac{\ln\varepsilon}{\sqrt{\varepsilon}} + O\left(\frac{1}{\sqrt{\varepsilon}}\right), \quad \varepsilon \to 0. \tag{F9}$$

Now the question is addressed what happens if within a layer of thickness $\eta = \varepsilon^k$ (i.e. $0 \leqslant \rho_1 \leqslant \varepsilon^k$), $(\sigma_y)_3$ is replaced by $(\sigma_y)_3 \cdot h(\rho_1)$, where $0 \leqslant h(\rho_1) \leqslant 1$.

Looking at the region $0 \leqslant \rho_1 \leqslant \varepsilon^k$ a generic integral in σ_1 looks like:

$$I \doteq \left|\int_0^{\varepsilon^{k-1}} \frac{\sqrt{x}\ln(\varepsilon x)\,h(\varepsilon x)\,\mathrm{d}x}{[1+x^2-2x\cos\theta_1\cos\phi_1]^{n/2}}\right| \leqslant \int_0^{\varepsilon^{k-1}} \frac{\sqrt{x}\,|\ln(\varepsilon x)|\,h(\varepsilon x)\,\mathrm{d}x}{[1-\cos^2\theta_1\cos^2\phi_1]^{n/2}} \tag{F10}$$

or

$$I \leqslant \frac{1}{[1-\cos^2\theta_1\cos^2\phi_1]^{n/2}} \int_0^{\varepsilon^k} \sqrt{x}\ln(\varepsilon x)\,\mathrm{d}x \sim -\tfrac{2}{3}\varepsilon^{3/2(k-1)}\ln(\varepsilon^k), \quad \varepsilon \to 0. \tag{F11}$$

For $k > 1$, eqn (F11) is subdominant with respect to the $\ln\varepsilon$ leading behaviour of the integral from 0 to ∞. This also means that, the other way around, if the loading is decreased within a layer of thickness $\varepsilon_{\mathrm{pres}}$, the leading behaviour of σ_1 will not change for $\varepsilon \geqslant \varepsilon_{\mathrm{pres}}^{1/k}$, $\varepsilon \ll 1$, $k > 1$. The same argument applies to σ_2.